Chaotic scattering and diffusion in the Lorentz gas

P. Gaspard and F. Baras
Centre for Nonlinear Phenomena and Complex Systems, Faculté des Sciences, Université Libre de Bruxelles, Campus Plaine, Code Postal 231, Boulevard du Triomphe, B-1050 Brussels, Belgium
(Received 3 November 1994)

A chaotic-scattering theory of diffusion in the Lorentz gas is presented. The scattering process is considered on disk scatterers of increasing sizes. In this way, chaotic and fractal properties of the scattering process are related to diffusion. A formula is obtained that gives the diffusion coefficient in terms of the Lyapunov exponent and the Hausdorff codimension of the fractal repeller of orbits trapped in the scatterer. Numerical results are presented that support our theoretical results.

PACS number(s): 05.45.+b, 05.60.+w, 03.80.+r

I. INTRODUCTION

The recent works obtained this last decade on deterministic chaos and dynamical system theory have shown the necessity to revise our understanding of irreversible processes in nonequilibrium statistical mechanics. In conventional statistical mechanical approaches to transport, only the macroscopic aspects of the irreversible processes are considered. In particular, scaling theory of hydrodynamics and diffusion have rigorously shown how the law of diffusion appears on large scales in mechanical systems such as the Lorentz gas. However, our knowledge is still very sparse about the way the microscopic reversible dynamics can accommodate macroscopically irreversible processes.

Recently, approaches have been proposed where the transport properties are related to the characteristic quantities of chaos such as the Lyapunov exponents, the Kolmogorov-Sinai (KS) entropy per unit time, the escape rate, and the fractal dimensions [1–9].

In this context, Evans, Cohen, and Morris [1] have considered a variant of the periodic Lorentz gas model with an electric field proposed by Moran and Hoover [2]. In order to avoid the kinetic energy to grow without bound, a special force acts on the particle to keep the kinetic energy constant. Accordingly, the system—although still reversible—no longer preserves phase space volumes so that the Liouville theorem is not obeyed. For this kind of dynamical system, the phase space contains an attractor as well as a distinct repeller (which is repelling in all directions). The trajectories converge to the attractor in the future and to the repeller in the past. Both the attractor and the repeller are fractal sets of zero Lebesgue measure. In this particular model, the transport properties of diffusion have been related to the sum of Lyapunov exponents and further results have been rigorously obtained by Chernov *et al.* [3]. However, the introduction of the special thermostat force is not compatible with the symplectic property of Hamiltonian systems.

This difficulty may be overcome by considering the conservative Lorentz gas under nonequilibrium boundary conditions as proposed by one of the authors and coworkers [4–9]. In this approach, developed independently of Refs. [1–3], the dynamics preserves the phase space volumes as well as the symplectic property, so that the fundamental properties of mechanics are not altered. Imposing nonequilibrium boundary conditions is equivalent to considering the scattering of particles on open configurations of the Lorentz gas. The diffusion coefficient can be shown to be proportional to the rate of escape of particles out of large scatterers because the escape dynamics is controlled by diffusion. Using dynamical system theory, the diffusion coefficient is related to the difference between the Lyapunov exponent and the KS entropy per unit time [4]. These quantities are defined for an invariant measure whose support is a fractal set of trajectories that are indefinitely trapped in the scattering region. This fractal set is a repeller of saddle-type with stable and unstable directions since trajectories can enter and exit the scattering region. In this regard, the fractal object considered in the scattering approach is different from the one considered in the thermostated-system approach.

Our purpose in this paper is to develop the escape-rate theory and the thermodynamic formalism for the study of diffusion and chaotic scattering in the open Lorentz gas. The thermodynamic formalism is constructed around the topological pressure of Ruelle from which the different characteristic quantities of chaos can be derived. In a previous paper [4], the diffusion coefficient has been given in terms of the Lyapunov exponent and the KS entropy or, equivalently, in terms of the Lyapunov exponent and the information dimension of the fractal repeller (for the definitions of these quantities, see [10]). In the present paper, we obtain a relation that connects directly the diffusion coefficient to the Hausdorff dimension and the Lyapunov exponent. This formula is derived from the previous results obtained by Gaspard and Nicolis [4]. Thereafter, we show how the diffusion coefficient can be calculated numerically in terms of the Hausdorff dimension of the fractal repeller. Our results provide evidence that diffusion has its origin in the phenomenon of chaotic scattering.

The paper is organized as follows. In Sec. II, the infinite and open Lorentz gases are defined and the prop-

1063-651X/95/51(6)/5332(21)/$06.00

erty of hyperbolicity is described. Sections III and IV are devoted to the infinite and open Lorentz gases, respectively. Section III on the infinite Lorentz gas gives a preamble to Sec. IV, which contains the main results of our paper. Indeed, several important points concerning the invariants measures and the pressure functions may be clarified by comparing the constructions and properties of the infinite and open configurations of the Lorentz gas. Our formula between the diffusion coefficient and the Hausdorff dimension is given in Sec. IV and numerical results are presented. Conclusions are drawn in Sec. V.

II. INFINITE AND OPEN CONFIGURATIONS OF THE LORENTZ GAS

A. Billiards

We consider classical billiards where a point particle undergoes elastic collisions on hard disks that are fixed in the plane, $\mathbf{r}=(x,y)$. The space between the disks forms the two-dimensional domain $\mathcal{D}$ of the billiard. All the hard disks have the same radius a ($a=1$ in this work). The centers of the disks belong to a triangular lattice

$$\mathbf{r}_c=m_c\mathbf{a}+n_c\mathbf{b}\ , \tag{2.1}$$

defined in terms of the fundamental translation vectors

$$\mathbf{a}=(d,0)\ ,\qquad \mathbf{b}=\left[\frac{1}{2}d,\frac{\sqrt{3}}{2}d\right]\ , \tag{2.2}$$

and where $(m_c,n_c)\in\mathbb{Z}^2$ are integers. Different billiards can be constructed depending on the set of pairs of integers that are selected.

1. The infinite configuration

If all the pairs of integers are selected, we fill the whole triangular lattice with hard disks. All the centers are occupied so that the billiard is invariant under the group of spatial translations generated by the vectors (2.1). Accordingly, the whole lattice can be mapped onto a so-called Wigner-Seitz cell with periodic boundary conditions [11]. The elementary Wigner-Seitz cell of this triangular lattice is an hexagon of area

$$A_{\rm WS}=|\mathbf{a}\times\mathbf{b}|=\frac{\sqrt{3}}{2}d^2\ , \tag{2.3}$$

(see Fig. 1) [11]. Under this construction, the position space forms a torus given by the quotient of the plane by the lattice: $\mathbb{T}^2=\mathbb{R}^2/\mathbb{Z}^2$.

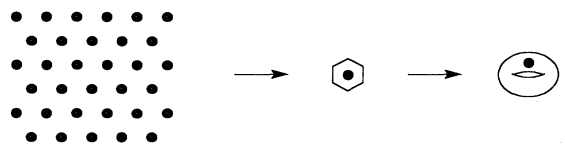

FIG. 1. Triangular lattice and its elementary Wigner-Seitz cell, as well as its topological equivalence with a torus.

The motion of the point particle in the infinite lattice is unbounded so that transport by diffusion is *a priori* possible. When the dynamics is reduced to the Wigner-Seitz cell, the position of the particle inside this cell must be supplemented by a lattice vector of the type (2.1) in order to determine the actual position of the particle in the infinite lattice. This lattice vector changes in discrete steps at each crossing of the border of the elementary Wigner-Seitz cell.

2. The open configurations of scattering type

Rather than filling the whole lattice with disks, we can fill only the lattice sides that are inside a closed curve C_R [4,9]. This curve can be defined in polar coordinates ($x=r\cos\alpha$, $y=r\sin\alpha$) by the equation $r=Rf(\alpha)$, which may be a circle, a hexagon, a square, etc. R is a parameter that varies from zero to infinity. Outside the curve C_R, the plane is empty of disks so that the point particle moves in a free motion from or to infinity. Accordingly, these open configurations define systems of scattering type (see Fig. 2). As $R\to\infty$, more and more disks are contained in the scatterer. The number of disks increases approximately as

$$N_R\approx\frac{A_R}{A_{\rm WS}}\ , \tag{2.4}$$

where A_R is the area of the domain enclosed in the curve C_R,

$$A_R=\frac{1}{2}R^2\int_0^{2\pi}[f(\alpha)]^2d\alpha\ , \tag{2.5}$$

and $A_{\rm WS}$ is the area (2.3) of the Wigner-Seitz cell.

We shall especially be concerned here by hexagonal scatterers for which the curve C_R is a hexagon reciprocal to the hexagon of the Wigner-Seitz cell (see Fig. 2). In this case, the number of disks inside C_R is

$$N_R=3n^2+3n+1,\quad \text{for } R=nd+\delta\ , \tag{2.6}$$

with $0<\delta\ll d$. For $R-\delta=d,2d,3d,4d,5d,6d,7d,8d,\ldots$, we have that the scatterer contains $N_R=7,19,37,61,91,127,169,217,\ldots$ disks [5]. If the particle belongs to the interior of the hexagon C_R, its position $\mathbf{r}$ satisfies the condition

$$\max\{|\mathbf{e}_1\cdot\mathbf{r}|,|\mathbf{e}_2\cdot\mathbf{r}|,|\mathbf{e}_3\cdot\mathbf{r}|\}<R\ , \tag{2.7}$$

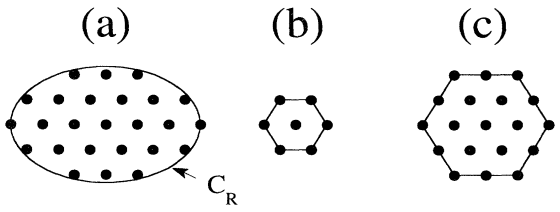

FIG. 2. Geometry of an open disk scatterer delimited (a) by a general curve C_R, (b) by a hexagonal curve $C_{R=d}$ selecting one shell of disk around the central one, and (c) by a hexagonal curve $C_{R=2d}$ selecting two shells.

in terms of the vectors that are normal to the sides of C_R: $\mathbf{e}_1=(0,1)$, $\mathbf{e}_2=(\sqrt{3}/2,1/2)$, and $\mathbf{e}_3=(\sqrt{3}/2,-1/2)$.

In the limit $R=\infty$, the open configurations of scattering type become identical to the infinite lattice. In this way, it is possible to make the connection between diffusion defined in the infinite lattice and the properties of the scattering process in finite configurations. From a physical point of view, this limit is natural since diffusion is studied in finite pieces of material in the laboratory. Diffusion is a property of bulk matter which is extrapolated from experiments on finite samples to a hypothetical infinite sample. Our purpose here is to study the detail of this limit in the case of the Lorentz gas.

B. The dynamics

Between two successive collisions, the motion of the point particle is determined by the free Hamiltonian

$$H=\frac{1}{2m}(p_x^2+p_y^2) , \tag{2.8}$$

where the momentum is related to the velocity by $\mathbf{p}=m\mathbf{v}$. At each collision, the velocity or momentum of the particle satisfies the law of reflection of geometric optics; the angle between the incident ray and the normal $\mathbf{n}_i$ at the point of impact is equal to the angle between the reflected ray and the normal (see Fig. 3).

This dynamics obeys the well-known variational principle that the total length of the path from the initial to the final positions is extremal for the actual trajectory,

$$\delta W(\{\mathbf{r}_i\})=0, \quad \text{with } W=\sum_{i=0}^{N} l(\mathbf{r}_i,\mathbf{r}_{i+1}) , \tag{2.9}$$

where $\mathbf{r}_i=(x_i,y_i)$ are the positions of the points of impact on the disks while $\mathbf{r}_0$ and $\mathbf{r}_{N+1}$ are the initial and final positions.

An efficient algorithm of integration of the trajectories of the billiard is based on vectorial analysis. The particle

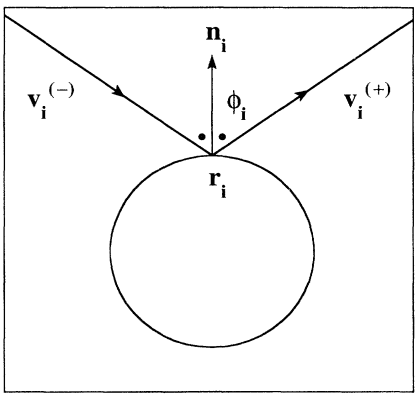

FIG. 3. Geometry of elastic collision: the point of impact $\mathbf{r}_i$; the normal at the point of impact $\mathbf{n}_i$, the ingoing and outgoing velocities, $\mathbf{v}_i^{(\pm)}$; the angle between the normal and the outgoing velocity ϕ_i.

velocities before and after the ith collision, we denote by $\mathbf{v}_i^{(-)}$ and $\mathbf{v}_i^{(+)}$, are related by the law of geometric optics

$$\mathbf{v}_i^{(+)}=\mathbf{v}_i^{(-)}-2[\mathbf{n}_i\cdot\mathbf{v}_i^{(-)}]\mathbf{n}_i , \tag{2.10}$$

while the trajectory between two successive collisions at times t_i and t_{i+1} is given by

$$\mathbf{r}(t)=\mathbf{r}_i+(t-t_i)\mathbf{v}_i^{(+)} . \tag{2.11}$$

If the next collision occurs on the disk centered at $\mathbf{r}_c$, the time of the collision is determined by solving the quadratic equation

$$[\mathbf{r}(t)-\mathbf{r}_c]^2=a^2 \tag{2.12}$$

or

$$A_i(t-t_i)^2+2B_i(t-t_i)+C_i=0 , \tag{2.13}$$

with

$$\begin{aligned} A_i&=(\mathbf{v}_i^{(+)})^2 ,\\ B_i&=\mathbf{v}_i^{(+)}\cdot(\mathbf{r}_i-\mathbf{r}_c) ,\\ C_i&=(\mathbf{r}_i-\mathbf{r}_c)^2-a^2 . \end{aligned} \tag{2.14}$$

The time of the next collision is, therefore, given by

$$t_{i+1}=t_i-\frac{B_i}{A_i}-\left[\left[\frac{B_i}{A_i}\right]^2-\frac{C_i}{A_i}\right]^{1/2} , \tag{2.15}$$

where the minus sign is chosen between both determinations of the square root because the collision occurs at the first intersection of the free trajectory (2.11) with the disk (2.12). The new position on the disk c is given by

$$\mathbf{r}_{i+1}=\mathbf{r}(t_{i+1}) , \tag{2.16}$$

while the normal at this point of impact is

$$\mathbf{n}_{i+1}=\frac{\mathbf{r}_{i+1}-\mathbf{r}_c}{|\mathbf{r}_{i+1}-\mathbf{r}_c|}=\frac{1}{a}(\mathbf{r}_{i+1}-\mathbf{r}_c) , \tag{2.17}$$

and the incident velocity at $\mathbf{r}_{i+1}$ is

$$\mathbf{v}_{i+1}^{(-)}=\mathbf{v}_i^{(+)} . \tag{2.18}$$

The outgoing velocity and the free flight after the collision are calculated identically starting again from Eq. (2.10). In this way, the complete trajectory can be calculated by recurrence.

A few remarks are necessary here about the geometry of the phase space. The Lorentz gas has two degrees of freedom so that its total phase space is four dimensional, (x,y,p_x,p_y). If the momentum is expressed in polar coordinates, $(p_x=p\cos\theta,\ p_y=p\sin\theta)$, the phase space coordinates may be taken as (x,y,θ,p).

Since energy is conserved, the four-dimensional phase space decomposes into a one-dimensional continuum of energy shells which are three dimensional, (x,y,θ). Moreover, due to the simple form of the Hamiltonian (2.8), the topology of the trajectories on the energy shells are similar to each other by a scaling of energy or velocity, $E=p^2/(2m)=(1/2)mv^2$. Accordingly, the

knowledge of the dynamics at a fixed velocity is enough to have the complete picture of the system. Here, we shall consider the energy shell with the velocity given in units of disk radius, $v=a=1$. If the trajectory has a total length L, the time of flight varies according to $t=L/v=L\sqrt{m/2E}$. For a unit velocity, time is then equal to the geometric length of the trajectories in position space. The trajectories can, therefore, be parametrized equivalently in terms of the time or the path length: $\Gamma_t=(x_t,y_t,\theta_t)=\Gamma_L$. Nevertheless, on the different energy shells, these trajectories are followed at different speeds.

C. Liouville invariant measure

Since we investigate statistical properties of the billiard dynamics, we introduce the Liouville invariant measure given by

$$d\mu_L=I_{\mathcal{D}}(x,y)\delta(H-E)dx\,dy\,dp_x dp_y\ , \tag{2.19}$$

in terms of the indicator function of the domain $\mathcal{D}$ defined by

$$I_{\mathcal{D}}(x,y)=\begin{cases}1, & \text{for } (x,y)\in\mathcal{D}\\ 0, & \text{otherwise}\ .\end{cases} \tag{2.20}$$

In polar coordinates where $dp_x dp_y=p\,dp\,d\theta$, the invariant measure (2.19) can be rewritten as

$$d\mu_L=mI_{\mathcal{D}}(x,y)\delta(p-\sqrt{2mE}\,)dp\,dx\,dy\,d\theta\ , \tag{2.21}$$

where we used the property of the Dirac distribution that

$$\delta\left[\frac{p^2}{2m}-E\right]=\frac{m}{p}\delta(p-\sqrt{2mE}\,)\ , \tag{2.22}$$

when $p\geq 0$. Equation (2.21) shows that the velocity angles and the positions are uniformly distributed according to the Liouville invariant measure with a density, $d\Gamma=dx\,dy\,d\theta$, on each energy shell.

The Liouville invariant measure (2.21) applies to every configuration of the Lorentz gas. This measure is not normalizable when the area of the domain $\mathcal{D}$ is infinite in the case of the infinite and open configurations. However, the measure is normalizable for the reduced dynamics in an elementary Wigner-Seitz cell where the area of the domain $\mathcal{D}$ takes a finite value. In this finite case, the Liouville invariant measure is a probability measure that defines the Gibbs microcanonical ensemble of equilibrium statistical mechanics. In the following Sec. IV, we shall introduce invariant probability measures that are relevant for the nonequilibrium mechanics of the open configurations of scattering type.

D. Finite or infinite horizon

In the infinite lattice configuration, different dynamical behaviors arise depending on the ratio of the distance d between the centers of the disks to the disk radius a. This ratio d/a determines the density of the disk lattice.

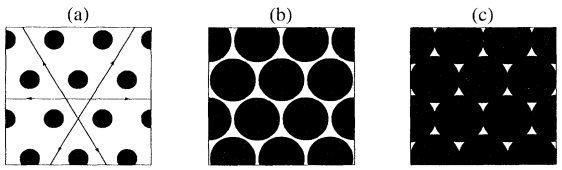

FIG. 4. (a) Triangular Lorentz gas in the infinite-horizon regime ($4a/\sqrt{3}<d$) with some of the special orbits traveling through the lattice without collisions, (b) Lorentz gas in the finite-horizon regime ($2a<d<4a/\sqrt{3}$), and (c) Lorentz gas in the localized regime ($\sqrt{3}a<d<2a$).

1. *Infinite-horizon regime*

In a low-density regime where the intercenter distance exceeds the critical value, $d>4a/\sqrt{3}$, the channels of the lattice are wide enough for an infinite number of disks to be reachable by free flight. In this case, the point particle can travel without any collision through the whole lattice along special trajectories. These special trajectories without collision exist only for velocity angles taking the discrete values $\theta=0$, $\pi/3$, $2\pi/3$, π, $4\pi/3$, and $5\pi/3$ so that they occupy a set of zero Liouville measure in phase space. This situation is referred to as the infinite-horizon configuration [see Fig. 4(a)] [12]. It is known that the diffusion coefficient is infinite in this regime ($\mathcal{D}=\infty$) [12].

2. *Finite-horizon regime*

For smaller intercenter distances, $2a<d<4a/\sqrt{3}$, only a finite set of at most six disks can be reached in free flight by the point particle when its velocity angle θ varies [see Fig. 4(b)]. Therefore, the horizon of the particle is now finite. In this finite-horizon regime, the diffusion coefficient in the lattice is known to be positive and finite ($0<\mathcal{D}<\infty$) [12].

3. *Localized regime*

When the distance between the centers is smaller than the diameter of the disks $\sqrt{3}a<d\leq 2a$, the disks partially overlap so that the point particle remains forever localized in closed domains delimited by three neighboring disks [see Fig. 4(c)]. In this case, unbounded motion is no longer possible and the diffusion coefficient vanishes ($\mathcal{D}=0$).

For $d\leq\sqrt{3}a$, the disks completely overlap so that the domain of billiard is empty and no dynamics is possible.

E. Hyperbolicity and Lyapunov exponents

The collision dynamics on the disks is defocusing, which induces a dynamical instability of the trajectories. This dynamical instability is characterized by the Lyapunov exponents that are the rates of exponential separations between a reference orbit and infinitesimally close orbits. The dynamics is said to be hyperbolic when each trajectory is exponentially unstable.

Since the dynamics is moreover symplectic and volume

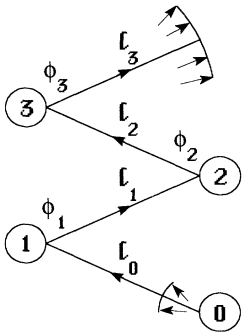

FIG. 5. Definition of the notation used in Eq. (2.26) for a typical trajectory and its accompanying expanding front (or horocycle).

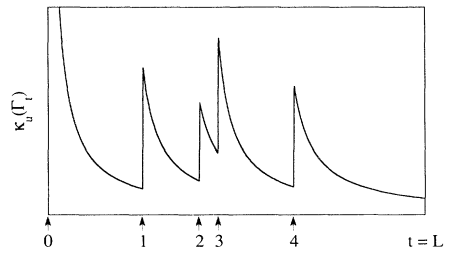

FIG. 6. Behavior of the front (horocycle) curvature $\kappa_u(\Gamma_t)$ versus the length of path $t=L$ for a typical trajectory escaping from the scatterer after four collisions.

preserving in the four-dimensional phase space, the Lyapunov exponents are $(\lambda,0,0,-\lambda)$ so that their sum is vanishing [10]. One of the Lyapunov exponents vanishes because of the absence of exponential separation in the direction of the flow, which is a general result for time-continuous systems. Another Lyapunov exponent corresponding to the direction perpendicular to the energy shell vanishes because of energy conservation. The dynamics of the Lorentz gas is not uniformly hyperbolic because the Lyapunov exponent may vary from one orbit to the other.

The positive Lyapunov exponent can be calculated by considering a front of particles accompanying the reference particle and issued from the same initial position (x,y) but with different initial velocity angles θ [12]. Because the dynamics is defocusing, this front is expanding (see Fig. 5). Locally on the reference orbit Γ_t, the front—called the unstable horocycle—is characterized by a curvature $\kappa_u(\Gamma_t)$ or equivalently, by a radius of curvature $1/\kappa_u$. The curvature depends on the time t of the orbit Γ_t. We now turn to the calculation of this curvature.

1. The horocycle curvature between two collisions

Around the initial position (x_0,y_0), the front is circular and its radius grows linearly with time t (or equivalently with time), so that

$$\kappa_u(\Gamma_t)=\frac{1}{t}, \quad \text{for } 0<t<l_0 \ . \tag{2.23}$$

Therefore, the curvature of the front diverges at the origin. At the first impact, the curvature is modified according to the geometry of the collision. After the ith collision, the front is locally equivalent to a circle of radius ρ_i. During the free motion to the next collision, the radius of this circle continues to grow linearly with the path length so that

$$\kappa_u(\Gamma_t)=\frac{1}{l+\rho_i}, \quad \text{for } 0<l<l_i \ , \tag{2.24}$$

where $l_i=|\mathbf{r}_{i+1}-\mathbf{r}_i|$ is the distance between the ith and the $(i+1)$th collisions and $t=l_0+l_1+\cdots+l_{i-1}+l$. We observe that the curvature of the horocycle decreases between each collision as depicted in Fig. 6.

If the particle escapes from the scatterer in free motion, the curvature continues to decrease to zero according to (2.24).

2. Changes of the horocycle curvature at collisions

Differentiating the collision rule (2.10) with respect to variations in the positions and velocities of the front particles at the ith collision, it has been shown elsewhere [12,13] that the front curvatures before and after the collision on a disk of radius a are related by

$$\frac{1}{\rho_i}=\kappa_u^{(+)}=\kappa_u^{(-)}+\frac{2}{a\cos\phi_i} \ , \tag{2.25}$$

where ϕ_i is the angle between the outgoing velocity of the reference orbit and the normal at the point of impact. Since $-\pi/2\le\phi\le+\pi/2$, we have that $\cos\phi\ge 0$. Consequently, the curvature increases at each collision, which is due to the defocusing dynamics of collisions on disks.

Combining the results (2.24) and (2.25), we obtain that the curvature of the front between the ith and $(i+1)$th collisions is given by the continuous fraction [12]

$$\kappa_u(\Gamma_t)=\cfrac{1}{l+\cfrac{1}{\cfrac{2}{a\cos\phi_i}+\cfrac{1}{l_{i-1}+\cfrac{2}{a\cos\phi_{i-1}}+\cdots+\cfrac{1}{\cfrac{2}{a\cos\phi_1}+\cfrac{1}{l_0}}}}} \tag{2.26}$$

where $0<l<l_i$ and $t=l_0+l_1+\cdots+l_{i-1}+l$.

3. Stretching factor and Lyapunov exponent

The local curvature (2.26) of the expanding front provides the rate of separation between the reference orbit and nearby orbits. Accordingly, the Lyapunov exponent per unit length of the orbit of initial condition Γ_0 is given by

$$\lambda(\Gamma_0)=\lim_{T_b\to\infty}\frac{1}{T_b-T_a}\int_{T_a}^{T_b}\kappa_u(\Gamma_t)dt\ . \tag{2.27}$$

Since the integral trivially diverges at $t=0$, we choose $T_a=l_0$. This choice has no consequence in the limit $T_b\to\infty$.

We also introduce the stretching factor of the expanding front between the path lengths T_a and T_b, which is defined by

$$\Lambda_{T_a,T_b}=\exp\int_{T_a}^{T_b}\kappa_u(\Gamma_t)dt\ . \tag{2.28}$$

Since the curvature is piecewise of the form (2.24) the integral can be performed analytically. For $T_b=l_0+l_1+\cdots+l_i$, we obtain [5]

$$\Lambda_{T_a,T_b}=[1+l_1C(\phi_1,l_0)][1+l_2C(\phi_2,l_1,\phi_1,l_0)]\times\cdots[1+l_iC(\phi_i,l_{i-1},\ldots,l_0)]\ , \tag{2.29}$$

where

$$C(\phi_i,l_{i-1},\ldots,l_0)=\frac{2}{a\cos\phi_i}+\frac{1}{l_{i-1}+\dfrac{1}{C(\phi_{i-1},l_{i-2},\ldots,l_0)}}\ , \tag{2.30}$$

with

$$C(\phi_1,l_0)=\frac{2}{a\cos\phi_1}+\frac{1}{l_0}\ . \tag{2.31}$$

We observe that each factor in Λ is greater than one so that we can expect an exponential growth of Λ with i. Therefore, if the orbit has infinitely many collisions occurring with a finite mean free path $\bar{l}$ between collisions, the Lyapunov exponent is positive. This is the case for every trajectory of the infinite lattice when the horizon is finite because we have that $(d-2a)\le l_i<\sqrt{3}d$. Accordingly, the finite-horizon regime is strictly hyperbolic since all the orbits have nonvanishing Lyapunov exponents.

On the other hand, when the horizon is infinite in the lattice configuration there exist special orbits without any collision so that their Lyapunov exponent vanishes. Therefore, the infinite-horizon regime is not strictly hyperbolic since orbits may have arbitrarily small Lyapunov exponents. However, the average Lyapunov exponent over the microcanonical invariant measure in a Wigner-Seitz cell turns out to be strictly positive, as we shall see in Sec. III.

In the open configurations of scattering type, most of the orbits escape from the scatterer after a finite number n of collisions. For $T_b=l_0+l_1+\cdots+l_n+l$, the stretching factor (2.29) grows linearly with l: $\Lambda\sim l$. Accordingly, the Lyapunov exponent of these orbits vanishes like $\lambda\sim\lim_{l\to\infty}\ln l/l=0$. However, we shall see in Sec. IV that there exist orbits that remain trapped between the disks and for which the Lyapunov exponent is nonvanishing.

III. INFINITE LORENTZ GAS

A. The billiard and its invariant measure

As we discussed in Sec. II the periodic Lorentz gas over a triangular lattice can be reduced to the motion of the point particle in a single Wigner-Seitz cell with periodic boundary conditions together with a lattice vector (2.1) changing in time by discrete jumps

$$\mathbf{r}_t^{(\text{lattice})}=\mathbf{r}_t^{(\text{cell})}+m_t\mathbf{a}+n_t\mathbf{b}\ . \tag{3.1}$$

The reduced dynamics takes place in a finite phase space. This dynamical system is known to be a Kolmogorov flow on each energy shell so that the mixing and ergodic properties are also satisfied [12]. Accordingly, almost every trajectory $\Gamma_t=(x_t,y_t,\theta_t)$ can be used to perform statistical averages. The time average of an observable, $A(x,y,\theta)$, is then equal to its phase space average [14]

$$\langle A\rangle_e=\int A(\Gamma)d\mu_e(\Gamma)=\lim_{T\to\infty}\frac{1}{T}\int_0^T A(\Gamma_t)dt\ , \tag{3.2}$$

which defines the equilibrium probability measure over the energy shell corresponding to the unit velocity

$$d\mu_e(x,y,\theta)=\frac{1}{\mathcal{Q}}dx\,dy\,d\theta\ . \tag{3.3}$$

The normalization constant is given by the range 2π of velocity angles multiplied by the area available to the particle in position space, i.e., the area of the Wigner-Seitz cell minus the area occupied by the disk

$$\mathcal{Q}=2\pi\left[\frac{\sqrt{3}}{2}d^2-\pi a^2\right]\ . \tag{3.4}$$

We remark that the ergodic procedure provided by the time average over a single trajectory has its origin in the finiteness of the phase space. We can use this result to calculate numerically several characteristic quantities of chaos in the Lorentz gas as well as the diffusion coefficient.

B. The average Lyapunov exponent

1. Definition

Using ergodicity, the average Lyapunov exponent can be obtained from the time average (2.27) for almost every initial condition Γ_0. Defining the stretching factor over a path length $T=L$ by

$$\Lambda_T(\Gamma_0)=\exp\int_{l_0}^{T}\kappa_u(\Gamma_t)dt\ , \tag{3.5}$$

the average Lyapunov exponent per unit length can be rewritten as [9]

$$\bar{\lambda}_e = \lim_{T\to\infty} \frac{1}{T} \ln \Lambda_T(\Gamma_0) \ . \tag{3.6}$$

By ergodicity, this time average is equivalent to an average (3.2) over the equilibrium measure (3.3)

$$\bar{\lambda}_e = \lim_{T\to\infty} \frac{1}{T} \int d\mu_e(\Gamma) \ln \Lambda_T(\Gamma) = \lim_{T\to\infty} \frac{1}{T} \langle \ln \Lambda_T \rangle_e \ . \tag{3.7}$$

However, there is a difference between the ways the formulas (3.6) and (3.7) are applied. In Eq. (3.6), a single trajectory is considered while in Eq. (3.7) the average is carried out over an ensemble of trajectories. The initial conditions may be chosen as successive points of a very long trajectory in order to have the initial conditions distributed according to the equilibrium measure.

2. Properties

We calculated numerically the average Lyapunov exponent for several intercenter distances d, as depicted in Fig. 7. As we mentioned earlier the average Lyapunov exponent is positive in the Lorentz gas even when the horizon becomes infinite at $d = 4a/\sqrt{3} = 2.3094a$. At this critical value, there is no apparent discontinuity in the behavior of the Lyapunov exponent as a function of the intercenter distance d.

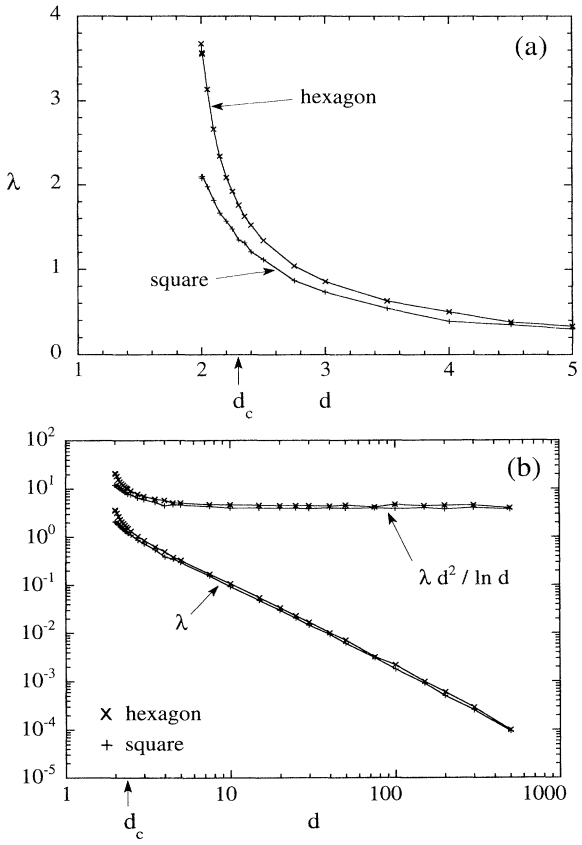

FIG. 7. (a) Average Lyapunov exponent versus the intercenter distance d for the dynamics in the Wigner-Seitz cell of the infinite Lorentz gas on triangular and square lattices. (b) Plot of $\bar{\lambda}_e d^2/\ln d$ versus d showing the dependency (3.10). The critical value of the transition from finite to infinite horizon, $d = d_c = 4a/\sqrt{3} = 2.3094a$, is marked to show the absence of consequence in the behavior of the Lyapunov exponent.

At larger values of d, the average Lyapunov exponent decreases monotonically to zero [see Fig. 7(a)]. This behavior has been explained as follows. When the disks are separated by a large distance d, the Lorentz gas is a dilute gas. The mean free path between collisions is determined by the density of disk, $n \sim d^{-2}$, and by the cross section, $s = 2a$, according to

$$\bar{l} = \frac{1}{ns} \sim \frac{d^2}{a} \ . \tag{3.8}$$

Over i collisions, the stretching factor (2.29) behaves essentially like

$$\Lambda_T \sim \left[\frac{\bar{l}}{a}\right]^i \sim \left[\frac{d^2}{a^2}\right]^i , \tag{3.9}$$

for large interdisk separations, $\bar{l} \gg a$. On average, there are about $i \sim L/\bar{l} \sim aL/d^2$ collisions over the path length $T = L$. Introducing these results in the definition (3.6), the average Lyapunov exponent behaves like [15,16]

$$\bar{\lambda}_e \sim \frac{a}{d^2} \ln \frac{d}{a} \ . \tag{3.10}$$

Figure 7(b) shows that $\bar{\lambda}_e d^2/\ln d$ is approximately constant as expected from (3.10).

For comparison, we also calculated the average Lyapunov exponent for the Lorentz gas in a square lattice. In this case, the Wigner-Seitz cell is a square. The reduced billiard is also known as the Sinai billiard [12]. In a square lattice, the horizon is always infinite so that diffusion is either absent or anomalous. However, this example shows that the average Lyapunov exponent may have a well-defined value even when the diffusion coefficient is infinite. This result corroborates the previous observation on the triangular lattice that the transition from the finite to the infinite horizon does not induce a change in the behavior of the average Lyapunov exponent. Figure 7 also shows that the average Lyapunov exponent is smaller for the square lattice than for the triangular lattice.

C. The pressure function and related quantities

1. Generalities

Bowen and Ruelle have introduced the pressure function into the thermodynamic formalism of dynamical systems [17–19]. The pressure function is a generalization of the Kolmogorov-Sinai entropy per unit time and was named pressure due to the analogy of its definition with the standard pressure of equilibrium statistical mechanics. The different characteristics quantities of chaos can be derived from the pressure function, as we show below.

In the case of a closed billiard in which averages can be calculated according to (3.2), we may define a pressure function according to

$$P_e(\beta)=\lim_{T\to\infty}\frac{1}{T}\ln\langle\Lambda_T^{1-\beta}\rangle_e$$
$$=\lim_{T\to\infty}\frac{1}{T}\ln\int d\mu_e(\Gamma)[\Lambda_T(\Gamma)]^{1-\beta}\ , \qquad (3.11)$$

where β is an exponent taking real values. Numerically, the average is carried out by integrating a very long trajectory, by cutting the trajectory into N segments of length T, by calculating $\Lambda_T^{1-\beta}$ for each segment, and by averaging to get

$$\langle\Lambda_T^{1-\beta}\rangle_e=\frac{1}{N}\sum_{j=1}^{N}[\Lambda_T(\Gamma_j)]^{1-\beta}\ . \qquad (3.12)$$

For a very long trajectory, the points, $\{\Gamma_j\}_{j=1}^N$, which are the initial conditions of the N segments, are distributed according to the ergodic equilibrium measure (3.3) and (3.4). Therefore, the above procedure satisfies the second equality in the definition (3.11).

The pressure function is known [17,18] to be a convex function that is monotonically decreasing or constant but never increasing. Moreover, in closed systems without escape, as is the case here for the reduced dynamics in a Wigner-Seitz cell, the pressure function vanishes when $\beta=1$,

$$P_e(1)=0 \quad \text{(closed systems)}\ . \qquad (3.13)$$

This result follows from the normalization of the probability measure, $\langle 1\rangle_e=1$.

A general result obtained by Bowen and Ruelle [19] which holds for hyperbolic systems is that the probability measure of a ball,

$$B(\Gamma_0,\varepsilon,T)=\{\Gamma_0':\text{dist}(\Gamma_t',\Gamma_t)\le\varepsilon,\ \forall t\in[0,T]\}\ , \qquad (3.14)$$

decreases exponentially with T as the inverse stretching factor of the reference orbit Γ_t

$$\mu_e(B(\Gamma_0,\varepsilon,T))\sim\frac{1}{\Lambda_T(\Gamma_0)} \quad \text{(closed systems)}\ . \qquad (3.15)$$

The ball (3.14) contains all the initial conditions Γ_0' such that the orbit issued from this initial condition remains within a distance ε of the reference orbit during the time T. "dist" denotes a distance defined in phase space. Using this property, the measure-theoretic pressure function we define here can be related to the topological pressure function defined by Bowen and Ruelle [17–19]. When the exponent β is set equal to zero, Eq. (3.12) becomes an average of the stretching factor, $\langle\Lambda_T\rangle_e$, in which Λ_T compensates the inverse stretching factor (3.15) coming from the measure so that the pressure function established a counting of the orbits of the system. In this case, it is known that the pressure is equal to the topological entropy per unit length in the system [20,21]

$$h_{\text{top}}=P_e(0)\ . \qquad (3.16)$$

The average Lyapunov exponent can be obtained from the pressure function by taking a derivative with respect to the exponent β,

$$\frac{d}{d\beta}P_e(\beta)=-\lim_{T\to\infty}\frac{1}{T}\frac{\langle\Lambda_T^{1-\beta}\ln\Lambda_T\rangle_e}{\langle\Lambda_T^{1-\beta}\rangle_e}\ . \qquad (3.17)$$

Setting $\beta=1$ and using the normalization of the measure $\langle 1\rangle_e=1$, we recover the definition (3.7) of the average Lyapunov exponent so that [21]

$$\bar{\lambda}_e=-P_e'(1)\ . \qquad (3.18)$$

According to Pesin's formula, which holds here because the system is hyperbolic and closed (no escape of particles), the KS entropy per unit length is equal to the average Lyapunov exponent [20–22],

$$\bar{\lambda}_e=h_{\text{KS}}(\mu_e) \quad \text{(closed systems)}\ . \qquad (3.19)$$

2. *The finite-horizon regime*

We calculated the pressure function using the definition (3.11) and (3.12). Figure 8 shows the pressure function versus the exponent β for $d=2.15a$ and $d=2.2a$ which are two configurations with a finite horizon since $d<4a/\sqrt{3}=2.3094a$. We observe that the pressure function is here nearly linear with a very small convexity that can be approximated by a Taylor expansion of the pressure around $\beta=1$,

$$P_e(\beta)=-\bar{\lambda}_e(\beta-1)+\tfrac{1}{2}P_e''(1)(\beta-1)^2+o((\beta-1)^2)$$
$$\text{(closed systems)}\ , \qquad (3.20)$$

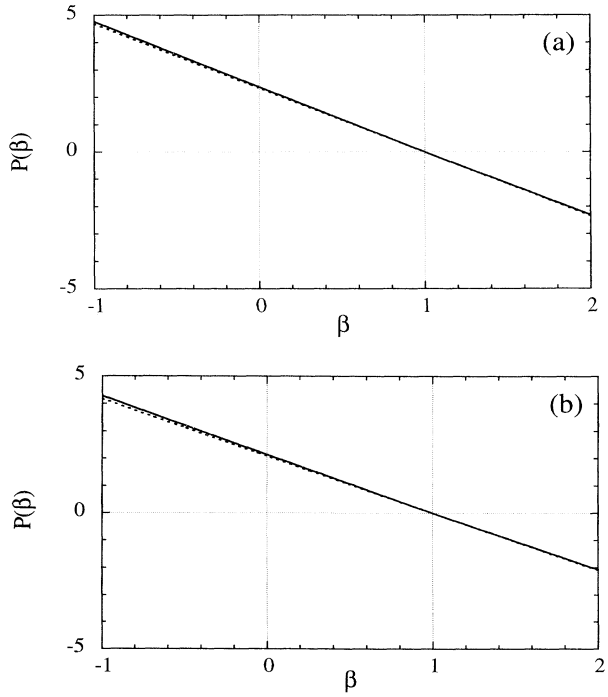

FIG. 8. Pressure function of the triangular infinite Lorentz gas calculated with (3.11) and (3.12) in the case of a finite horizon for (a) $d=2.15a$ and (b) $d=2.2a$. The dashed line is a straight line tangent to the pressure at $\beta=1$, the slope of which is $-\bar{\lambda}_e$.

TABLE I. Characteristic quantities for closed triangular Lorentz gas.

d/a	$\bar{\lambda}_e = h_{KS}(\mu_e)$	$\sigma_e^2 = P_e''(1)$	h_{top}
2.01	3.56	0.54	3.68
2.15	2.34	0.71	2.38
2.2	2.09	0.67	2.14
3	0.857		0.90
7.5	0.170		0.19
10	0.107		0.12

where $o(z)$ denotes a quantity such that $\lim_{z\to 0} o(z)/z = 0$ [23]. The expansion (3.20) is based on the assumption that the second derivative of the pressure function is at least continuous [$P_e(\beta) \in \mathcal{C}^2$].

The second derivative of the pressure can be interpreted as the variance σ^2 of the Lyapunov exponents since

$$P_e''(1) = \lim_{T\to\infty} \frac{1}{T} \langle (\ln \Lambda_T - \langle \ln \Lambda_T \rangle_e)^2 \rangle_e = \sigma_e^2 , \quad (3.21)$$

where $\ln\Lambda_T$ can be considered as a Lyapunov exponent over a time T.

The different characteristic quantities of chaos are given in Table I for different intercenter distances d.

3. *The infinite-horizon regime*

When the horizon becomes infinite a new feature appears in the pressure function which is due to the special orbits with zero Lyapunov exponent we mentioned in Sec. II D 1. In this regime, a point particle may travel without collision over a distance L if its velocity is directed in the small angles of order L^{-1} in the channels of the lattice. Therefore, the probability for the particle to have no collision over the time $T = L$ decreases like L^{-1}. Accordingly, the average (3.12) contains a few terms for which $\Lambda_T = 1$. Figure 9 shows a histogram of the values of $(1/T)\ln\Lambda_T$ obtained from an ensemble of 5000 trajectories of time $T = 10\,000$ when $d = 10a$. Although small, the number of trajectories with $\ln\Lambda_T = 0$ is nevertheless present, which has important consequences on the pressure function.

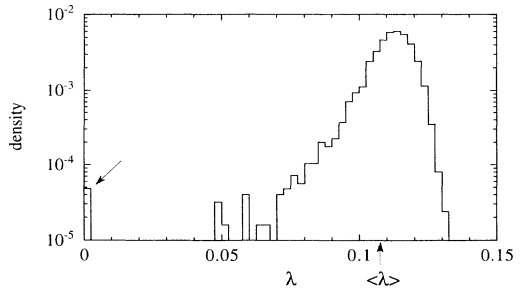

FIG. 9. Histogram of the Lyapunov exponents of the triangular infinite Lorentz gas $d = 10a$ and $a = 1$, calculated as $\lambda = (1/T)\ln\Lambda_T$ with $T = 10\,000$ for 5000 trajectories. $\langle\lambda\rangle = \bar{\lambda}_e = 0.107$ is the value of the average Lyapunov exponent.

Indeed, when $\beta > 1$, the sum (3.12) is dominated by the few terms equal to one which are due to the vanishing Lyapunov exponents. The other terms decrease to zero as $T \to \infty$. Accordingly, the pressure function vanishes for $\beta > 1$. On the other hand, for $\beta < 1$, the sum is dominated by the terms associated with unstable orbits with nonvanishing Lyapunov exponents so that the pressure function is then nontrivial. A consequence of the nonhyperbolicity when the horizon is infinite is, therefore, the appearance of a discontinuity in the derivative of the pressure function (see Fig. 10). This discontinuity can be interpreted as a phase transition [20,21,24]. It is known [17,18] that there exists an invariant measure μ_β associated with each value of β, which is of the form

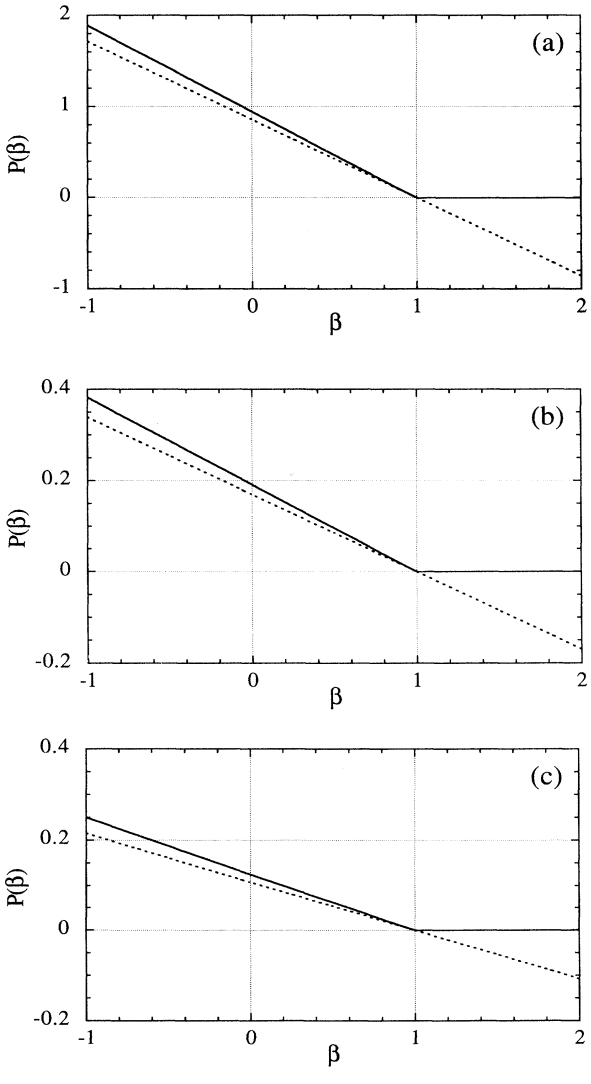

FIG. 10. Pressure function of the triangular infinite Lorentz gas calculated with (3.11) and (3.12) for (a) $d = 3a$, (b) $d = 7.5a$, and (c) $d = 10a$. The dashed line is a straight line tangent to the pressure at $\beta = 1$, the slope of which is $-\bar{\lambda}_e$.

$$\mu_\beta(B(\Gamma_0,\varepsilon,T)) \propto \frac{1}{[\Lambda_T(\Gamma_0)]^\beta} \quad \text{(closed systems)}, \tag{3.22}$$

instead of (3.15). In the particular case where $\beta=1$, the invariant measure $\mu_{\beta=1}=\mu_e$ coincides with the equilibrium measure (3.3). For the values $\beta<1$, the invariant measure μ_β is distributed over the random and unstable trajectories of the system. Accordingly, these states μ_β correspond to a disordered or chaotic phase. On the other hand, for $\beta>1$, the invariant measure is distributed only over the special regular orbits with zero Lyapunov exponents, so that these states correspond to an ordered phase.

Because of the discontinuity, the average Lyapunov exponent is now given by the left-hand derivative of the pressure at $\beta=1$ in Eq. (3.18). The right-hand derivative gives the average Lyapunov exponent in the ordered phase, which is vanishing. Since the pressure function is no longer regular at $\beta=1$ when the horizon is infinite, we remark that the expansion (3.20) is no longer applicable as such.

In the following, we shall restrict ourselves to the finite-horizon case for which diffusion is normal with a finite diffusion coefficient.

D. The diffusion coefficient

The diffusion coefficient is defined by Einstein's formula according to [25]

$$\mathcal{D}=\lim_{t\to\infty}\frac{1}{4t}\langle(\mathbf{r}_t^{(\text{lattice})}-\mathbf{r}_0^{(\text{lattice})})^2\rangle . \tag{3.23}$$

Since the system is mixing, the average can be taken over any smooth enough density of initial conditions. In the limit $t\to\infty$, the nonequilibrium average is equivalent to the equilibrium average for initial conditions in the Wigner-Seitz cell. Using the reduction (3.1) of the dynamics to the Wigner-Seitz cell, the diffusion coefficient becomes

$$\mathcal{D}=\lim_{t\to\infty}\frac{1}{4t}\langle(m_t\mathbf{a}+n_t\mathbf{b}+\mathbf{r}_t^{(\text{cell})}-\mathbf{r}_0^{(\text{cell})^2}\rangle_e , \tag{3.24}$$

where the average is taken over the equilibrium measure (3.3). In the triangular lattice, diffusion is isotropic so that the diffusion coefficient can be calculated independently from the x or y projection of the position vector $\mathbf{r}_t$. Using the Green-Kubo (GK) formula [26], the diffusion coefficient can be expressed in terms of the velocity autocorrelation of the particle

$$\mathcal{D}_{\text{GK}}=\frac{1}{2}\int_0^\infty\langle\mathbf{v}_t\cdot\mathbf{v}_0\rangle_e dt . \tag{3.25}$$

This method has been used by Machta and Zwanzig [27] to calculate numerically the diffusion coefficient of the triangular Lorentz gas as a function of the intercenter distance d.

Moreover, these authors have obtained an approximation for the diffusion coefficient in the limit of small gaps $(d-2a)$ between the disks. In this case, the particle spends a long time bouncing in the triangular cells of the lattice with rare transitions from cell to cell. Accordingly, the transition rate can be calculated assuming a quasiequilibrium in each triangular cell, yielding [27]

$$\mathcal{D}_{\text{th}}\simeq v\frac{d^2}{\pi(d^2\sqrt{3}-2\pi a^2)}(d-2a) , \tag{3.26}$$

which vanishes as $d\to 2a$ as $\mathcal{D}_{\text{th}}\simeq 1.97v(d-2a)$. However, this formula does not apply when the interdisk gaps are large, in particular, near the transition between the finite and infinite horizons at $d=4a/\sqrt{3}$.

For $d>4a/\sqrt{3}$, the diffusion coefficient is infinite as we already mentioned [12]. The values of the diffusion coefficient obtained by Machta and Zwanzig [27] with (3.25) and (3.26) are reported in Table II for comparison with our results on the open Lorentz gas in Sec. IV.

TABLE II. Diffusion coefficients of the triangular Lorentz gas versus the intercenter distance d/a in the first column. The second column gives the average Lyapunov exponent $\bar{\lambda}_e$ calculated with (3.6). The third column gives the theoretical diffusion coefficient $\mathcal{D}_{\text{th}}$ of Machta and Zwanzig [Eq. (3.26)]. The fourth column gives the numerical values $\mathcal{D}_{\text{GK}}$ of Machta and Zwanzig obtained with the Green-Kubo formula (3.25). The fifth column gives the diffusion coefficient $\mathcal{D}_{\text{esc}}$, we calculated using the first-passage method and Eqs. (4.18) and (4.19). The sixth column gives the diffusion coefficient obtained from the Hausdorff dimension of the fractal repeller thanks to our new formula (4.58).

d/a	$\bar{\lambda}_e$	$\mathcal{D}_{\text{th}}$	$\mathcal{D}_{\text{GK}}$	$\mathcal{D}_{\text{esc}}$	$\mathcal{D}_{\text{fractal}}$
2.002		0.00387	0.0036±0.0003		
2.01	3.56	0.0180	0.017±0.002	0.0169±0.0009	
2.04		0.0573	0.052±0.002		
2.05	3.14	0.0672		0.0585±0.0004	
2.06		0.0760	0.069		
2.1	2.66	0.104	0.10±0.01	0.096±0.007	0.09
2.15	2.34	0.128	0.14	0.134±0.004	0.13
2.2	2.09	0.147	0.18	0.161±0.004	0.17
2.25	1.92	0.162		0.205±0.003	0.21
2.3	1.76	0.175	0.25±0.01	0.25±0.01	0.25
>2.3094		∞			

IV. OPEN LORENTZ GAS

A. Escape-time function and escape rate

As described in Sec. II, we consider the scattering of a point particle on a set of regularly ordered hard disks forming a hexagon.

Since the system is open, particles escape to infinity. The trajectories Γ_t issued from the initial conditions have a diffusive motion in the scatterer until the border of the scatterer is reached (see Fig. 11). Thereafter, the trajectory escapes in free motion to infinity. Let us recall that the border of the scatterer is delimited by the curve C_R.

Although most trajectories escape from the scatterer, there exist trajectories that remain trapped inside the scatterer. They play a very important role because they control the escape dynamics. For instance, the periodic orbits bouncing on the line between the centers of two nearby disks remain trapped in the scatterer for $t\to\pm\infty$.

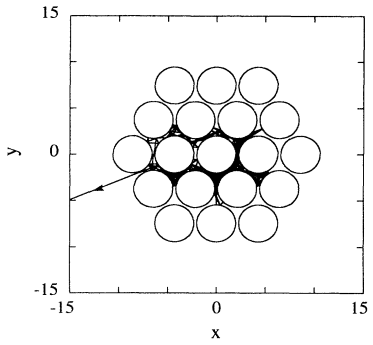

FIG. 11. Trajectory of a particle escaping after 366 collisions from a hexagonal scatterer of Lorentz type formed by two shells of disks with $R=2d$, $d=2.15a$, and $a=2$. The initial condition is located on the central disk at an angle $\alpha=\pi/4$.

Beside the periodic orbits, there also exist nonperiodic orbits that are forever trapped in the scatterer as soon as the scatterer contains three disks [9]. The trapped orbits are all unstable with strictly positive Lyapunov exponents and they form a fractal set of zero Lebesgue measure in phase space. Each trapped orbit has a stable and an unstable manifold that are associated with the negative and positive Lyapunov exponents. Time-reversal symmetry maps the stable manifolds onto the unstable ones. Because the trapped orbits are unstable, the set of trapped orbits is repelling and is accordingly called the fractal repeller $\mathcal{F}_R$ [4,9,20,28]. The existence of this fractal repeller is typical of chaotic-scattering processes. Many recent works have been devoted to chaotic scattering in small systems [29]. Here, we investigate the consequences of chaotic scattering when the system becomes spatially extended.

Evidence for the fractal repeller is provided by the escape-time function [9]. For each trajectory of initial condition $\Gamma_0=(x_0,y_0,\theta_0)$, we can calculate the time at which the border C_R is crossed, which we call the escape time $\mathcal{T}_{C_R}(\Gamma_0)$. The escape-time function is finite for almost all trajectories since they escape in a finite time. However, the escape time is infinite for trajectories that are trapped by the fractal repeller. Trapping occurs if the initial condition belongs to an indefinitely trapped orbit or to its stable manifold. The escape-time function has, therefore, singularities on the fractal set formed by the closure of the stable manifolds of the fractal repeller: $\mathrm{cl}(W_s(\mathcal{F}_R))$.

Figure 12 shows the escape-time function in the open Lorentz gas for which $R=2d$ and $d=2.15a$. We see that the singularities occupy a very important fraction of initial conditions in spite of the fact that they are of zero Lebesgue measure. This phenomenon is due to the fact that the Hausdorff dimension of the fractal set is close to one. This observation is fundamental for the following considerations. The deterministic character of the escape process is hidden in the existence of the windows of continuity in the escape-time function where the function is

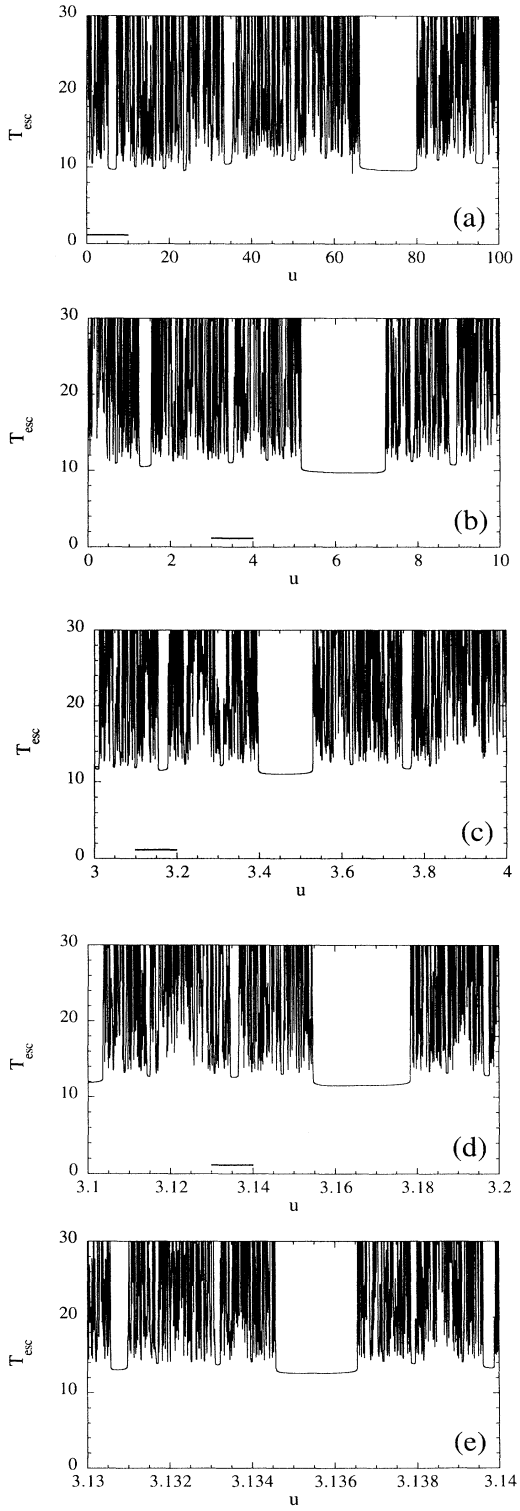

FIG. 12. Escape-time function for the scatterer $R=2d$, $d=2.15a$, $a=1$, for initial conditions $\alpha=\pi/4$ and $\phi=\theta-\alpha=\pi/2-\pi u\times10^{-10}$, showing the intervals of continuity that form the signature of the deterministic dynamics on these extremely small scales: (a) $u\in[0,100]$, (b) $u\in[0,10]$, (c) $u\in[3,4]$, (d) $u\in[3.1,3.2]$, and (e) $u\in[3.13,3.14]$. The comparison between the different intervals lets the scaling behavior appear.

regular in some intervals of initial conditions. For these initial conditions, the trajectories follow nearby paths that bounce on the same disks and exit through the same two disks. However, we observe that the widths of these windows of continuity are extremely small, which restricts considerably the range of deterministic considerations.

The escape dynamics can be further characterized by statistical quantities. Let us consider a gedanken experiment where a set of N_0 initial conditions, $\{\Gamma_0^{(j)}\}$, is chosen inside the scatterer according to an initial measure ν_0

$$d\nu_0(\Gamma)=\lim_{N_0\to\infty}\frac{1}{N_0}\sum_{j=1}^{N_0}\delta(\Gamma-\Gamma_0^{(j)})d\Gamma\ . \tag{4.1}$$

The number of particles N_T remaining inside the scatterer decreases monotonically with time T. The particles that escape after a predetermined time T belong to the set of initial conditions for which the escape time is larger than T:

$$\Upsilon_R(T)=\{\Gamma_0\in C_R: T<\tau_{C_R}(\Gamma_0)\}=\bigcap_{0<t<T}\Phi^{-t}(C_R)\ , \tag{4.2}$$

where Φ^t denotes the mapping induced by the flow over a time t in phase space. In the long-time limit, this set only contains the closure of the stable manifolds of the fractal repeller which are limited to C_R:

$$\lim_{T\to+\infty}\Upsilon_R(T)=\mathrm{cl}(W_s(\mathcal{F}_R))\cap C_R\ . \tag{4.3}$$

The population decay of the initial ensemble ν_0 is, therefore, given by

$$\lim_{N_0\to\infty}\frac{N_T}{N_0}=\nu_0(\Upsilon_R(T))=\int_{\Upsilon_R(T)}d\nu_0(\Gamma_0)\ . \tag{4.4}$$

We note that the limit $N_0\to\infty$ is essential to define a smooth function of time over $0<T<+\infty$ since N_T shows large statistical fluctuations when $N_T<10$ and drops to zero after a finite time.

The decay curve (4.4) may be exponential or slower than exponential in general systems [9]. Since the limit set (4.3) is a fractal with a zero ν_0 measure, the decay curve vanishes as $T\to+\infty$. We expect that the decay is exponential because all the trapped orbits are exponentially unstable. An escape rate is, therefore, defined according to [10]

$$\gamma=\lim_{T\to+\infty}\frac{(-)}{T}\ln\nu_0(\Upsilon_R(T))\ . \tag{4.5}$$

The escape rate is a further characteristic quantity of the system in the case of open systems. We also expected that the escape rate is independent of the initial measure ν_0 at the condition that this later is smooth enough.

B. The nonequilibrium invariant measure

The assumed independency of the escape rate (4.5) is very important for the following considerations and constitutes the analog of the ergodic hypothesis in the case of open systems.

Our purpose now is to construct an invariant measure for open systems. Contrary to the closed systems of Sec. III, we are not allowed to take an arbitrary initial condition, to run the trajectory for a long time, and to take time averages. Indeed, almost all the trajectories escape from the scatterer so that the above procedure would give useless results. Therefore, we cannot define the average of an observable A by standard ergodicity using the time average (3.2). On the contrary, we expect that the meaningful information is contained in the trajectories that are forever trapped inside the scatterer. Accordingly, we have to construct an invariant measure whose support is the fractal repeller $\mathcal{F}_R$.

For scattering systems, we define the average of an observable $A(\Gamma)$ which is smooth enough and whose support is contained inside C_R by selecting the orbits of the initial ensemble ν_0 that remain inside the scatterer over the time T and by taking the time average of A over the time T,

$$\mu_{\mathrm{ne}}(A)=\lim_{T\to+\infty}\lim_{N_0\to\infty}\frac{1}{N_T}\sum_{j=1}^{N_T}\frac{1}{T}\int_0^T A(\Phi^t\Gamma_0^{(j)})dt\ . \tag{4.6}$$

In Eq. (4.6), the sum extends over the N_T particles $\{\Gamma_0^{(j)}\}$ of the statistical ensemble ν_0 which are still in the scatterer at time T. This averaging can be rewritten in terms of the initial measure ν_0 as

$$\mu_{\mathrm{ne}}(A)=\int A(\Gamma)\lim_{T\to+\infty}\frac{1}{T}\int_0^T dt\frac{1}{\nu_0(\Upsilon_R(T))}I_{\Upsilon_R(T)}(\Phi^{-t}\Gamma)\times d\nu_0(\Phi^{-t}\Gamma)\ , \tag{4.7}$$

where $I_{\mathcal{E}}(\Gamma)$ denotes the indicator function of the set $\mathcal{E}$ in phase space. In this way, we obtain the nonequilibrium invariant probability measure

$$d\mu_{\mathrm{ne}}(\Gamma)=\lim_{T\to+\infty}\frac{1}{T}\int_0^T dt\frac{1}{\nu_0(\Upsilon_R(T))}I_{\Upsilon_R(T)}(\Phi^{-t}\Gamma)\times d\nu_0(\Phi^{-t}\Gamma)\ , \tag{4.8}$$

which has the fractal repeller $\mathcal{F}_R$ as support. This measure is normalized to one because of the denominator. This measure amounts to carry out a statistics on the set of N_T initial conditions which are still in the scatterer C_R at time T. In the limits $N_0\to\infty$ and $T\to+\infty$, these transient trajectories approach closer and closer to the fractal repeller $\mathcal{F}_R$. As a consequence, the probability measure is invariant on the repeller in the limit $T\to+\infty$.

We note that this invariant measure becomes identical with the microcanonical equilibrium invariant measure (3.3) (after an appropriate renormalization) in the limit where the scatterer has an infinite extension and becomes closed. Thanks to the measure (4.6)–(4.8), we are able to extend the thermodynamic formalism from bounded to open systems and to rigorously define Lyapunov exponents, entropies, and fractal dimensions.

Let us add that the results (3.14) and (3.15) generalize

to the nonequilibrium invariant measure defined here. We define a ball around the initial condition Γ_0 of a trajectory whose escape time exceeds $T[\mathcal{T}(\Gamma_0)>T]$ as in (3.14),

$$B(\Gamma_0,\varepsilon,T)=\{\Gamma_0':\mathrm{dist}(\Gamma_t',\Gamma_t)\leq\varepsilon,\ \forall t\in[0,T]\}\ . \tag{4.9}$$

The measure of this ball decreases exponential with T as the inverse stretching factor of the reference orbit Γ_t,

$$\mu_{\mathrm{ne}}(B(\Gamma_0,\varepsilon,T))\sim\frac{\exp(\gamma T)}{\Lambda_T(\Gamma_0)}\quad\text{(open systems)}\ , \tag{4.10}$$

with the extra factor $\exp(\gamma T)$ which is due to the normalization of the probability measure μ_{ne}.

C. Phenomenology of the escape process

When the size R of the scatterer becomes large enough with respect to the intercenter distance d, the motion in the scatterer is essentially controlled by the diffusion equation

$$\partial_t f=\mathcal{D}\nabla^2 f\ , \tag{4.11}$$

where $f=f(x,y)$ is the density of particles around the position (x,y). This diffusion equation holds when the horizon of the Lorentz gas is finite so that $0<\mathcal{D}<\infty$. At the border C_R where the particles escape from the scatterer, the density should be considered as being equal to zero because the particles disappear from the diffusion process by escaping to infinity. Therefore, the time evolution of the particle density is obtained by solving the diffusion equation with the absorbing boundary condition

$$f|_{C_R}=0\ . \tag{4.12}$$

We may expect an exponential decay of the probability density, $f\sim\exp(-\gamma t)$, where γ is a decay rate. We assume that the density evolves in time according to

$$f(x,y;t)=\sum_{n=1}^{\infty}c_n\exp(-\gamma_n t)\varphi_n(x,y)\ , \tag{4.13}$$

where the constants c_n are determined by the initial density. Accordingly, the decay rates γ_n are obtained by an eigenvalue problem for the Helmholtz equation

$$(\mathcal{D}\nabla^2+\gamma_n)\varphi_n=0,\quad\text{with }\varphi_n|_{C_R}=0\ , \tag{4.14}$$

where φ_n are the associated eigenfunctions.

Using the scaling $(x,y)\to(Rx,Ry)$, the eigenvalue equation (4.14) becomes

$$(\nabla^2+\chi_n^2)\tilde{\varphi}_n=0,\quad\text{with }\tilde{\varphi}_n|_{C_{R=1}}=0\ , \tag{4.15}$$

where $\tilde{\varphi}_n(x,y)=\varphi_n(Rx,Ry)$. The phenomenological decay rates are then given by

$$\gamma_n=\mathcal{D}\left[\frac{\chi_n}{R}\right]^2\ . \tag{4.16}$$

We note that the preceding phenomenological description holds only in the limit of a large scatterer ($R\to\infty$) and for the lowest eigenvalues in order to guarantee that the corresponding wavelengths remain large with respect to the size of the lattice cells: $2\pi R/\chi_n\gg d$. Indeed, the wavelengths of the higher eigenvalues may become shorter than the lattice cells, in which case we expect a discrepancy between the phenomenological description and the actual Liouvillian dynamics. Hereafter, we shall use the result (4.16) in its domain of validity for the Lorentz gas, i.e., for $n=1$ and $R\to\infty$.

Equations (4.13) and (4.16) describe the escape of a statistical ensemble of N_0 particles out of the scatterer. At long times ($t\to\infty$), the escape is dominated by the smallest decay rate, γ_1. The number N_t of particles still present inside the scatterer at time t is given in terms of the density according to

$$N_t\simeq N_0\int_{C_R}dx\,dy\,f(x,y;t)\sim N_0\exp(-\gamma_1 t)\ . \tag{4.17}$$

We obtain the result that the first phenomenological decay rate γ_1 gives the escape rate previously defined by (4.5) for the scatterer C_R:

$$\gamma=\mathcal{D}\left[\frac{\chi_1}{R}\right]^2+o(R^{-2})\ , \tag{4.18}$$

in the limit $R\gg d$.

For the hexagonal scatterers, the first eigenvalue is [30]

$$\chi_1=2.674\,95,\quad\text{(hexagon)}\ . \tag{4.19}$$

Figure 13 gives the first eigenvalue χ_1 for different shapes of scatterers.

As a consequence of the previous observations, we can determine the diffusion coefficient by this escape method, which is alternative to the methods based on the Einstein and Green-Kubo formulas. We refer to this method as a first-passage method because the diffusion coefficient is related to the statistics of the times of the first passage for the diffusing particles [4,5].

In the ensemble ν_0 of initial conditions we consider, the positions of the different particles are identical and located at the point $x_0=y_0=a\sin(\pi/4)$ on the border of the central disk of the scatterer. The initial velocity angles are uniformly distributed in the interval $-\pi/4\leq\theta\leq 3\pi/4$. Figure 14 shows the decay of the number N_t of particles for a scatterer with $R=2d$ and $d=2.15a$. We observe without ambiguity that the decay is exponential after the usual transients, which allows us to obtain the escape rate γ with an accuracy of 1%. The escape

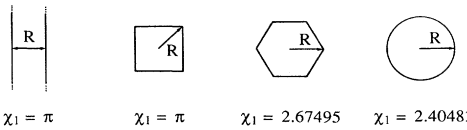

FIG. 13. The constant χ_1 appearing in Eq. (4.18) for the smallest eigenvalue of the problem (4.15) in the different geometries of the absorbing boundary. For the hexagon, cf. Ref. [30]. For the circle, χ_1 is given by the first zero of the Bessel function $J_0(x)$.

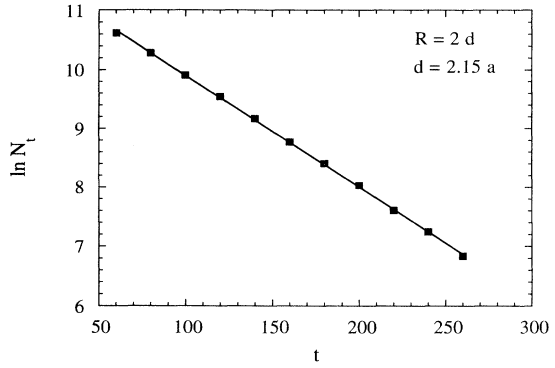

FIG. 14. $\ln N_t$ versus the time t for a typical escape rate simulation at $R=2d$, $d=2.15a$, and $a=2$.

rates for different scatterers of increasing sizes R/d but fixed ratio d/a are then collected in Fig. 15 where it is possible to determine the diffusion coefficient $\mathcal{D}=\mathcal{D}_{\rm esc}$ using (4.18) and (4.19). The diffusion coefficients $\mathcal{D}_{\rm esc}$ are obtained by extrapolation from the escape rates for sizes varying from $R=4d$ to $R=10d$. The error is mainly due to the uncertainties in the different extrapolations taken from the escape-rate values at pairs of odd or even values of R/d. Repeating the numerical calculation for different ratios d/a, we obtain finally the diffusion coefficients in Table II and Fig. 16 where we compare the results of our escape method with those obtained by the Green-Kubo formula [27]. We see that the agreement is excellent and that the accuracy of the escape method is comparable to the accuracy of the Green-Kubo method.

D. Average Lyapunov exponent

For the open configuration, we may define the average Lyapunov exponent over the invariant measure (4.8) according to

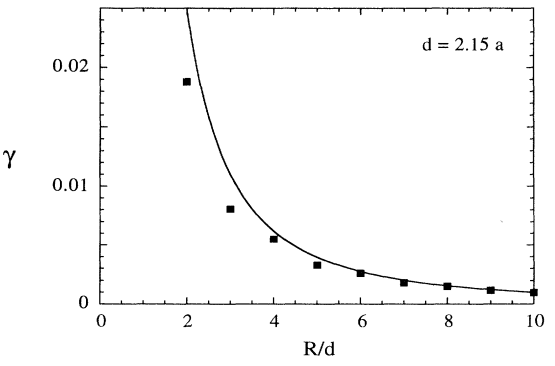

FIG. 15. Escape rate versus the size R/d for $d=2.15a$ and $a=2$ (dots) and compared with the prediction of (4.18) and (4.19) with the theoretical diffusion coefficient (3.26).

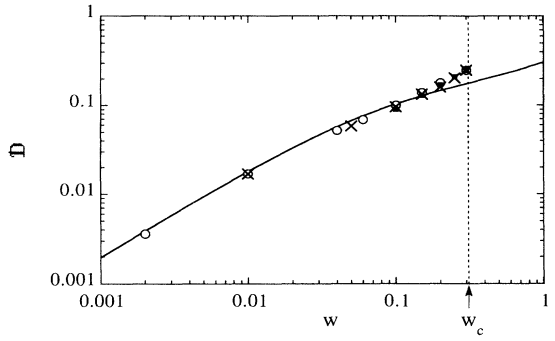

FIG. 16. Logarithm of the diffusion coefficients versus the logarithm of the gap size $w=(d/a)-2$ with $a=1$. The solid line is the theoretical diffusion coefficient of Machta and Zwanzig (3.26). The numerical results obtained by Machta and Zwanzig using the Green-Kubo formula are shown by circles. The diffusion coefficients obtained in the present work with the first-passage method are presented by crosses. The diffusion coefficients obtained in the present work from the Lyapunov exponents and the Hausdorff codimensions are presented by squares. The transition from finite to infinite horizon at $w_c=(4/\sqrt{3})-2=0.3094$ is shown by the dashed line.

$$\bar{\lambda}=\int \kappa_u(\Gamma)d\mu_{\rm ne}(\Gamma)\ , \tag{4.20}$$

which corresponds to taking the average of the logarithms of the stretching factors at time T for all the N_T particles still in the scatterer at time T,

$$\bar{\lambda}=\lim_{T\to+\infty}\lim_{N_0\to\infty}\frac{1}{T}\frac{1}{N_T}\sum_{j=1}^{N_T}\ln\Lambda_T(\Gamma_0^{(j)})\ . \tag{4.21}$$

Here, we adopted a different but similar average based on the histogram of the logarithm of the stretching factors of the particles at their escape times: $\ln\Lambda_{\mathcal{T}^{(i)}}(\Gamma_0^{(i)})$ for $i=1,2,\ldots,N_0$. The histogram is composed of classes of events defined according to the escape times by $t<\mathcal{T}^{(i)}<t+\Delta t$ where $t=n\Delta t$, and Δt is an interval of time. Each class contains a number of events given by $\Delta N_t=N_t-N_{t+\Delta t}$. The average of the logarithms of these stretching factors in each class of the histogram is defined by

$$\langle\ln\Lambda_{\mathcal{T}}\rangle_{(t;\Delta t)}=\frac{1}{\Delta N_t}\sum_{j=1}^{\Delta N_t}\ln\Lambda_{\mathcal{T}^{(j)}}(\Gamma_0^{(j)})\ . \tag{4.22}$$

The average Lyapunov exponent is given by the following expression [5]:

$$\bar{\lambda}=\lim_{t\to+\infty}\lim_{N_0\to\infty}\frac{1}{t}\langle\ln\Lambda_{\mathcal{T}}\rangle_{(t;\Delta t)}\ , \tag{4.23}$$

which is statistically equivalent to Eqs. (4.20) and (4.21). In the limit $t\to\infty$, Eq. (4.23) becomes independent of the constant Δt entering the definition of the histogram.

Using the same averaging procedure, we can also define the variance of the Lyapunov exponent as

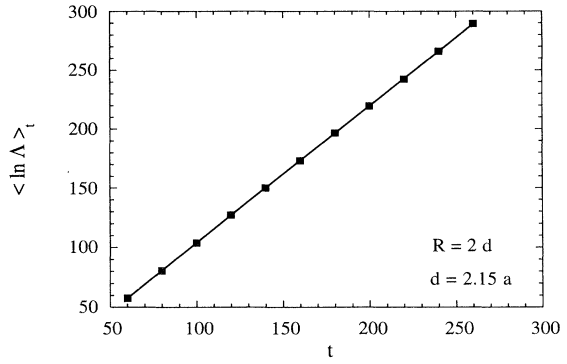

FIG. 17. $\langle \ln\Lambda \rangle_t$ versus time t for $R=2d$, $d=2.15a$, and $a=2$. The slope is the Lyapunov exponent $\bar{\lambda}$.

$$\sigma^2 = \lim_{t\to\infty} \lim_{N_0\to\infty} \frac{1}{t} \langle (\ln\Lambda_T - \langle \ln\Lambda_T \rangle_{(t;\Delta t)})^2 \rangle_{(t;\Delta t)} , \tag{4.24}$$

in analogy with (3.21).

We numerically evaluated the Lyapunov exponent for open configurations of the Lorentz gas with Eq. (4.23). Figure 17 shows the behavior of $\langle \ln\Lambda_T \rangle_{(t;\Delta t)}$ as a function of time. The slope gives us the average Lyapunov exponent $\bar{\lambda}$ with a very good accuracy of the order of 0.1%. We observed that the dependence of the Lyapunov exponents on the size R of the scatterer is below the numerical error. The numerical values obtained for open configurations are approximately equal to the values of the Lyapunov exponents of the closed Lorentz gas given in Sec. III (see Table III). These values appear to be equal within the numerical error. This seems to also be the case for the variances of the Lyapunov exponent (compare Tables I and III). We note that the small differences between the values of σ^2 in Tables I and III may be due to differences in the methods we used to obtain them. In Table I, we numerically differentiated the pressure function while in Table III, we directly calculated the variance with (4.24). Although we do not expect an exact equality between the values of these quantities in the closed and open configurations, we nevertheless expect that these quantities become equal in the limit of large scatterers $R\to\infty$. This convergence is rapid since an approximate equality already holds for $R=2d$ or $R=3d$. As a consequence, the Lyapunov exponents of the closed and open configurations have a similar dependency on the intercenter distances d/a, which we described in Sec. III B 2.

E. The pressure function and the thermodynamic formalism

1. Definition

Our purpose in this subsection is to develop the thermodynamic formalism starting from a definition of the pressure function in open configurations. In this way, we can relate different quantities together and obtain the generalized fractal dimensions with, in particular, the information and Hausdorff dimensions [20,21,31].

In order to define a pressure function that is applicable to open systems of scattering type, we adapt the definition (3.11) for closed systems to the new invariant measure we define with (4.6)–(4.8) for open systems. We proceed in analogy with the definition of the average Lyapunov exponent (4.20) and (4.21). In this way, the pressure function is defined by

$$P(\beta) = \lim_{T\to+\infty} \frac{1}{T} \ln \int_{\Upsilon_R(T)} [\Lambda_T(\Gamma)]^{1-\beta} d\nu_0(\Gamma) , \tag{4.25}$$

which corresponds to a statistics over the N_T particles still in the scatterer at time T,

$$P(\beta) = \lim_{T\to+\infty} \lim_{N_0\to\infty} \frac{1}{T} \ln \frac{1}{N_0} \sum_{j=1}^{N_T} [\Lambda_T(\Gamma_0^{(j)})]^{1-\beta} , \tag{4.26}$$

but with a normalization with respect to the initial number N_0 of particles. Equation (4.26) can be rewritten in terms of the same normalization as in Eq. (4.21),

TABLE III. Chaotic properties of the fractal repeller in the triangular Lorentz gas for three different scatterers. The escape rate γ, the average Lyapunov exponent $\bar{\lambda}$, and the Hausdorff dimension d_H are obtained by independent calculations based on (4.5), (4.23), and (4.45), respectively. The KS entropy, the information dimension d_I, and the codimensions, c_H and c_I, are derived using (4.32), (4.40), (4.43), and (4.44), respectively.

	$R=2d$		$R=3d$
Quantity	$d=2.15a$	$d=2.2a$	$d=2.2a$
$\bar{\lambda}$	2.32	2.08	2.080±0.002
$\sigma^2=P''(1)$	0.75	0.70	0.702±0.006
γ	$3.76\times10^{-2}\pm6\times10^{-4}$	4.4×10^{-2}	$1.92\times10^{-2}\pm10^{-4}$
$h_{KS}=\bar{\lambda}-\gamma$	2.28	2.04	2.061±0.002
$d_I=h_{KS}/\bar{\lambda}$	0.984	0.979	0.991 ± 10^{-3}
$c_I=1-d_I$	0.016	0.021	0.009 ± 10^{-3}
d_H	0.984	0.980	0.9903
$c_H=1-d_H$	0.016	0.020	0.0097

$$P(\beta)=-\gamma+\lim_{T\to+\infty}\lim_{N_0\to\infty}\frac{1}{T}\ln\frac{1}{N_T}\sum_{j=1}^{N_T}[\Lambda_T(\Gamma_0^{(j)})]^{1-\beta}\ , \tag{4.27}$$

where the escape rate γ now appears because of (4.5).

An equivalent definition uses the histogram method of (4.22) and (4.23):

$$P(\beta)=-\gamma+\lim_{t\to+\infty}\lim_{N_0\to\infty}\frac{1}{t}\ln\langle\Lambda_T^{1-\beta}\rangle_{(t;\Delta t)}\ . \tag{4.28}$$

2. Properties

Several properties follow from the previous definitions. In particular, the average Lyapunov exponent is given by minus the derivative of the pressure function at $\beta=1$ as with (3.18) [21],

$$\bar{\lambda}=-P'(1)\ . \tag{4.29}$$

Taking the second derivative of the pressure with respect to β at $\beta=1$ yields the variance (4.24) of the Lyapunov exponents so that (3.21) holds here also,

$$\sigma^2=P''(1)\ . \tag{4.30}$$

However, differences with respect to closed systems arise due to the extra term $-\gamma$ in Eq. (4.27). In particular, the escape rate is given here by minus the pressure evaluated at $\beta=1$ [20,21],

$$\gamma=-P(1)\ \text{(open systems)}\ . \tag{4.31}$$

The pressure function is schematically represented in Fig. 18. It is a convex function that is either monotonically decreasing or constant [17–19].

A KS entropy per unit time can be defined for the invariant measure by the standard procedure that considers partitions into cells of the phase space around the repeller [14]. The KS entropy per unit time is defined as the supremum of the partition entropies per unit time over all possible partitions [14]. The KS entropy per unit time is known to be related to the difference between the average Lyapunov exponent and the escape rate [9,10,20,21,23],

$$h_{\rm KS}(\mu_{\rm ne})=\bar{\lambda}-\gamma\ \ \text{(open systems)}\ , \tag{4.32}$$

which generalizes Pesin's formula to open systems. The origin of this formula can be understood on the basis of the result (4.10). According to the Shannon-Breiman theorem [14], the KS entropy is given by the decay rate of the measure, $\mu_{\rm ne}(B(\Gamma_0,\varepsilon,T))\sim\exp[-Th_{\rm KS}(\mu_{\rm ne})]$. In the right-hand side of (4.10), the inverse stretching factor decreases at a rate given by the average Lyapunov exponent, $\Lambda_T(\Gamma_0)^{-1}\sim\exp(-\bar{\lambda}T)$. Hence, the factor $\exp(\gamma T)$ in Eq. (4.10) explains the presence of the escape rate in (4.32).

F. The partial generalized fractal dimensions

In order to further characterize the fractal repeller, we need to calculate the fractal dimensions. We consider a Poincaré section of the flow that intersects transversally with the repeller as shown in Fig. 19. Let us take a line $\mathcal{L}$ across the stable manifolds of the fractal repeller. The intersections of this line with the stable manifolds of the fractal repeller is another fractal with generalized dimensions taking their values in the interval $0\le d_q\le 1$. These dimensions are referred to as partial dimensions in contrast to the dimensions of the fractal repeller itself in the three-dimensional phase space, which belong to the interval $0\le D_q\le 3$ and which are related to the partial dimensions by $D_q=2d_q+1$.

The line $\mathcal{L}$ can be taken as the support of the ensemble

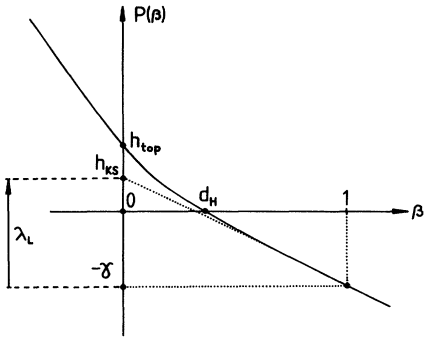

FIG. 18. Schematic behavior of the pressure function in the case of an open system.

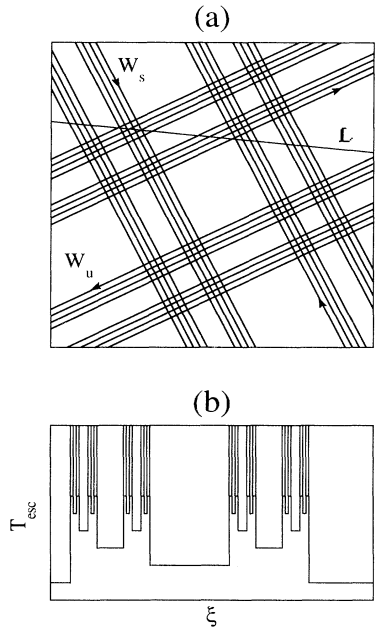

FIG. 19. (a) Schematic shape of the stable and unstable manifolds of the fractal repeller with an intersecting line $\mathcal{L}$. (b) Schematic escape-time function along the line $\mathcal{L}$ of curvilinear coordinate ξ.

ν_0 of initial conditions (4.1). The escape-time function can be calculated on this line. Since the escape-time function has singularities on a fractal, the set of initial conditions for which the escape time is larger than T is composed of many small intervals that form a covering of the fractal repeller. The widths of the intervals of the covering are approximately given by the inverse of the stretching factors up to time T,

$$l_i \sim \frac{1}{\Lambda_T(\Gamma_0^{(j)})} , \tag{4.33}$$

for trajectories of initial conditions $\{\Gamma_0^{(j)}\}$ in the initial ensemble ν_0. On the other hand, using the result (4.10), the probabilities of these intervals l_j are given by

$$p_i \sim \frac{\exp(\gamma T)}{\Lambda_T(\Gamma_0^{(j)})} , \tag{4.34}$$

with the normalization $\sum_{i=1}^{M} p_i = 1$.

Hasley *et al.* have shown how to define the generalized fractal dimensions associated with a measure like $\mu_{\rm ne}$. In the limit $T \to \infty$, the partial generalized dimensions d_q are determined by the condition that the following quantity must remain of the order of one [31],

$$\sum_{i=1}^{M} \frac{p_i^q}{l_i^{(q-1)d_q}} \sim 1 \quad \text{for } M \to \infty , \tag{4.35}$$

where M is the number of intervals in the covering of the fractal. The left-hand side of (4.35) can be rewritten as a statistical average over the measure $\mu_{\rm ne}$

$$\sum_{i=1}^{M} p_i \frac{p_i^{q-1}}{l_i^{(q-1)d_q}} = \left\langle \frac{p_i^{q-1}}{l_i^{(q-1)d_q}} \right\rangle . \tag{4.36}$$

Introducing the results (4.33) and (4.34) in Eqs. (4.35) and (4.36), the generalized dimensions must satisfy

$$\exp[(q-1)\gamma T] \langle \Lambda_T^{(q-1)(d_q-1)} \rangle_{(t;\Delta t)} \underset{t \to +\infty}{\sim} 1 , \tag{4.37}$$

where we adopted the histogram method of average as in (4.28). Using the relation (4.28) to the pressure, we obtain the result that the generalized dimensions are given as the roots of the following equations [20,21]:

$$P(q+(1-q)d_q) = -q\gamma . \tag{4.38}$$

When $q=0$, the generalized dimension is equal to the Hausdorff dimension, $d_0 = d_H$, which is given as the root of the pressure, itself [20,21],

$$P(d_H) = 0 . \tag{4.39}$$

Since the escape rate is nonvanishing in open systems, the Hausdorff dimension is smaller than unity so that the repeller does not completely fill the phase space as already anticipated. When the scatterer becomes very large, the escape rate vanishes according to (4.18) so that Hausdorff dimension approaches the unit value in this limit $R \to \infty$. Before elaborating on this result, let us mention other useful results.

The information dimension is given when $q=1$, $d_I = d_1$. Differentiating (4.38) with respect to q and setting $q=1$, Young's formula is obtained [32]:

$$d_I = 1 - \frac{P(1)}{P'(1)} = 1 - \frac{\gamma}{\bar{\lambda}} = \frac{h_{\rm KS}}{\bar{\lambda}} , \tag{4.40}$$

where we used (4.32). Accordingly, the information dimension is directly related to the KS entropy and the average Lyapunov exponent. Let us also mention the inequality [31],

$$d_I \leq d_H , \tag{4.41}$$

coming from the convexity of the pressure function. The $f(\alpha)$ spectrum [31] can also be derived by a Legendre transform of the generalized dimension d_q [20,21]. Since the pressure function is slightly convex when the horizon of the Lorentz gas is finite we expect a nontrivial $f(\alpha)$ function so that the repeller is a multifractal. However, the pressure function is so close to a straight line that the multifractal character is very small and the repeller is very close to a uniform fractal. For these reasons, the difference between the information and the Hausdorff dimension should be small also.

Because the partial generalized dimensions are close to the value one when the scatterer is large, it is convenient to introduce the codimensions [5] that are the defects of the partial dimensions with respect to one,

$$c_q = 1 - d_q . \tag{4.42}$$

In particular, we have the Hausdorff and the information codimensions

$$c_H = 1 - d_H , \tag{4.43}$$

$$c_I = 1 - d_I . \tag{4.44}$$

The codimensions also belong to the interval, $0 \leq c_q \leq 1$.

G. The Maryland algorithm for the Hausdorff codimension

The Hausdorff codimension can be obtained using the following numerical algorithm developed by the group of Maryland [33]. An ensemble of pairs of initial conditions separated by ε is considered along the line of support of ν_0 (see Fig. 19). The pair is said to be uncertain if there is a singularity of the escape-time function between both initial conditions, i.e., if the corresponding trajectories follow paths that differ by the successive impacts on the disks. If we associate to each trajectory a symbolic sequence, $\omega_0\omega_1 \ldots \omega_n$, which gives the labels of the disks on which the successive collisions occur, the pair is certain if the symbolic sequences corresponding to both initial conditions are identical. When the pair is certain, they belong to an interval of continuity of the escape-time function where they are not separated by a singularity (see Fig. 19). On the other hand, the symbolic sequences are different when the pair is uncertain. The fraction $f(\varepsilon)$ of uncertain pairs in the initial ensemble ν_0 is known to behave like

$$f(\varepsilon) \sim \varepsilon^{c_H} . \tag{4.45}$$

A derivation of this result can be found elsewhere [33,34].

We used this algorithm in order to obtain an estima-

tion of a fractal dimension that would be independent of the escape rate and of the Lyapunov exponent. To apply the Maryland algorithm, we need to integrate two nearby trajectories and to compare their properties. However, if both trajectories, $(\mathbf{r}_i,\mathbf{v}_i^{(\pm)})$ and $(\mathbf{r}_i',\mathbf{v}_i^{(\pm)'})$, are integrated by the method described in Sec. II B, we face the difficulty that the differences between their coordinates cannot be smaller than the rounding error of the computer used, namely $\varepsilon > 10^{-15}$ in simple precision and $\varepsilon > 10^{-30}$ in double precision on a Cray computer. This restriction would prevent one from determining the Hausdorff dimension of large scatterers as seen below.

To avoid this restriction, we simultaneously integrate the reference trajectory $(\mathbf{r}_i,\mathbf{v}_i^{(\pm)})$ together with the difference between the perturbed and the reference trajectories,

$$(\Delta\mathbf{r}_i,\Delta\mathbf{v}_i^{(\pm)})=(\mathbf{r}_i'-\mathbf{r}_i,\mathbf{v}_i^{(\pm)'}-\mathbf{v}_i^{(\pm)}) . \tag{4.46}$$

The reference trajectory is integrated by Eqs. (2.10)–(2.18). The difference (4.46) is integrated by equations given by the finite differences of Eqs. (2.10)–(2.18). In particular, the difference on the reflected velocity is

$$\Delta\mathbf{v}_i^{(+)}=\Delta\mathbf{v}_i^{(-)}-2[\mathbf{n}_i'\cdot\mathbf{v}_i^{(-)'}]\Delta\mathbf{n}_i -2[\mathbf{n}_i'\cdot\Delta\mathbf{v}_i^{(-)}]\mathbf{n}_i-2[\Delta\mathbf{n}_i\cdot\mathbf{v}_i^{(-)}]\mathbf{n}_i . \tag{4.47}$$

The difference in the time of flight between both collisions is

$$\Delta(t_{i+1}-t_i)=-\Delta B_i-\frac{(B_i'+B_i)\Delta B_i-\Delta C_i}{\sqrt{B_i'^2-C_i'}+\sqrt{B_i^2-C_i}} , \tag{4.48}$$

with

$$\Delta B_i=\mathbf{v}_i^{(+)'}\cdot\Delta\mathbf{r}_i+\Delta\mathbf{v}_i^{(+)}\cdot(\mathbf{r}_i-\mathbf{r}_c) , \qquad \Delta C_i=(\mathbf{r}_i'+\mathbf{r}_i-2\mathbf{r}_c)\cdot\Delta\mathbf{r}_i , \tag{4.49}$$

and where we supposed a velocity of unit magnitude, $A_i=1$. The difference in the new positions at the next collision is given by

$$\Delta\mathbf{r}_{i+1}=\mathbf{v}_i^{(+)'}\Delta(t_{i+1}-t_i)+\Delta\mathbf{v}_i^{(+)}(t_{i+1}-t_i)+\Delta\mathbf{r}_i . \tag{4.50}$$

The differences in the normal vectors at the points of impact and in the incident velocities are obtained as

$$\Delta\mathbf{n}_{i+1}=\frac{1}{a}\Delta\mathbf{r}_{i+1} , \qquad \Delta\mathbf{v}_{i+1}^{(-)}=\Delta\mathbf{v}_i^{(+)} . \tag{4.51}$$

In this way, both trajectories of the pair can be calculated by recurrence. The integration of Eqs. (4.47)–(4.51) has to be stopped as soon as the reference and the perturbed trajectories have collisions on different disks, i.e., as soon as one of the square roots in the denominator of Eq. (4.48) becomes undefined.

In the present work, the differences on the initial conditions are taken as

$$\Delta\mathbf{r}_0=a(\cos(\alpha_0+\varepsilon)-\cos(\alpha_0),\sin(\alpha_0+\varepsilon)-\sin(\alpha_0)) =2a\sin\left[\frac{\varepsilon}{2}\right]\left[-\sin\left[\alpha_0+\frac{\varepsilon}{2}\right],\cos\left[\alpha_0+\frac{\varepsilon}{2}\right]\right] , \qquad \Delta\mathbf{v}_0^{(+)}=\mathbf{0} , \tag{4.52}$$

where α_0 varies between 0 and $\pi/6$.

This method allows us to reach the value $\varepsilon\simeq 10^{-300}$, which is the minimum decimal power available on standard FORTRAN compilers. Since the dynamics is unstable, the difference $(\Delta\mathbf{r}_i,\Delta\mathbf{v}_i^{(\pm)})$ is expected to grow so that the exponent does not decrease below 10^{-300}. In this way, the Hausdorff dimension can be obtained for large scatterers where c_H is very small.

H. The diffusion coefficient in terms of the Hausdorff codimension

We are now in position to relate the diffusion coefficient to the quantities characterizing chaotic scattering.

In a previous work, Gaspard and Nicolis [4] have combined the results (4.18) and (4.32) to obtain the formula

$$\mathcal{D}=\lim_{R\to\infty}\left[\frac{R}{\chi_1}\right]^2[\bar{\lambda}(\mathcal{J}_R)-h_{\mathrm{KS}}(\mathcal{J}_R)] , \tag{4.53}$$

where the averages are taken over the invariant measure (4.6)–(4.8) defined on the fractal repeller $\mathcal{J}_R$. Equation (4.53) can be expressed in terms of the information codimension using Young's formula (4.40),

$$\mathcal{D}=\lim_{R\to\infty}\left[\frac{R}{\chi_1}\right]^2\bar{\lambda}(\mathcal{J}_R)c_I(\mathcal{J}_R) . \tag{4.54}$$

Now, we would like to obtain another formula similar to (4.54) but where the Hausdorff codimension appears instead of the information codimension. We assume that the horizon of the Lorentz gas is finite so that the pressure function does not present a phase transition in the closed configuration limit $R\to\infty$. As in (3.20), we assume that the second derivative of the pressure function is continuous at $\beta=1$ to obtain

$$P(\beta)=-\gamma-\bar{\lambda}(\beta-1)+\tfrac{1}{2}P''(1)(\beta-1)^2+o[(\beta-1)^2] \quad \text{(open systems)} \tag{4.55}$$

instead of (3.20). Using (4.39) and (4.43), we obtain

$$c_H=\frac{\gamma}{\bar{\lambda}}-P''(1)\frac{\gamma^2}{2\bar{\lambda}^3}+o(\gamma^2)=c_I-\frac{P''(1)}{2\bar{\lambda}}c_I^2+o(c_I^2) . \tag{4.56}$$

Using the result (4.18), we infer that both the information and the Hausdorff codimensions have a similar leading behavior as a function of the size R of the scatterer

$$\left.\begin{matrix}c_H\\ c_I\end{matrix}\right\}=\frac{\mathcal{D}}{\bar{\lambda}}\left[\frac{\chi_1}{R}\right]^2+o(R^{-2}) . \tag{4.57}$$

Taking the limit $R\to\infty$, we finally obtain the diffusion coefficient in terms of the Hausdorff codimension

$$\mathcal{D}=\lim_{R\to\infty}\left[\frac{R}{\chi_1}\right]^2\bar{\lambda}(\mathcal{J}_R)c_H(\mathcal{J}_R)\ , \tag{4.58}$$

which is the analog of (4.54). We may expect a similar behavior in terms of other generalized codimensions.

I. Discussion and numerical results

The Hausdorff dimensions have been calculated using the algorithm of the Maryland group based on the fraction of uncertain pairs of orbits. As discussed earlier, the availability of the Hausdorff dimension is based on the possibility to resolve the escape-time function into the intervals of continuity separated by the singularities (see Fig. 12). When the size R of the scatterer increases, the time spent by the particles in the scatterer increases in average as $t\sim\gamma^{-1}\sim R^2$ and the stretching factors of the individual trajectories as $\Lambda\sim\exp(\lambda t)\sim\exp(cR^2)$ where c is a positive constant. A simple argument shows that the intervals of continuity are of the order of Λ^{-1}. We conclude that the determination of the Hausdorff dimension requires one to consider extremely small differences of the order of $\varepsilon\sim\exp(-cR^2)$ in the formula (4.45). As a consequence, the Hausdorff dimension becomes difficult to determine when the size of the scatterer increases.

We applied the algorithm we proposed in Sec. IV G to several open scatterers of the Lorentz gas. The fraction of uncertain pairs of orbits is plotted in Fig. 20 for $d=2.2a$. We observe the dramatic decrease in orbit separation that is required to reach the scaling behavior when the size R increases. This astonishing observation shows how fast the deterministic character of the diffusion process disappears on minute scales as the size of the scatterer increases. A linear regression in the scaling domain where Eq. (4.45) applies provides us with a determination of the Hausdorff codimension c_H. In Table III, we reported the values of the different characteristic quantities we calculated for a few scatterers. We remark that the information and Hausdorff codimensions

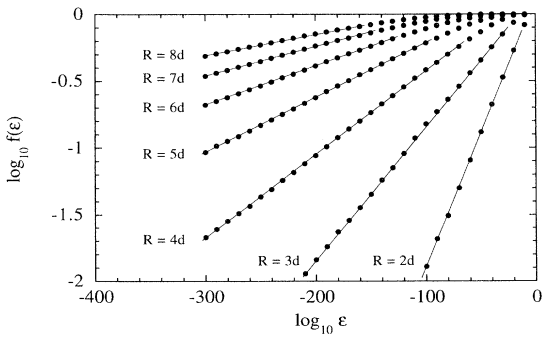

FIG. 20. Log-log plot of the fraction $f(\varepsilon)$ of uncertain pairs of points versus the separation ε for the scatterers from $R=2d$ to $R=8d$ with an interdisk distance of $d=2.2a$ ($a=1$). Note the dramatic shift of the scaling regime towards extremely small separations when R increases. Each point is obtained with a statistical ensemble of 10^4 initial conditions.

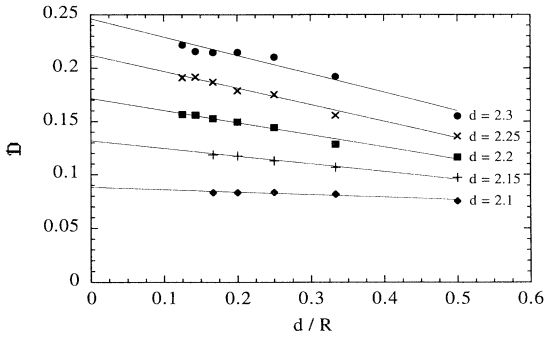

FIG. 21. Left-hand member of Eq. (4.58) versus d/R. The diffusion coefficient is determined by linear extrapolation assuming that the left-hand member of (4.58) behaves like $\mathcal{D}_{\text{fractal}}+C/R$ where C is a constant. The numerical values so obtained are reported in Table II.

are nearly equal within the numerical error.

Figure 21 shows the values of the right-hand member of Eq. (4.58) for increasing values of the size R which behaves like $\mathcal{D}_{\text{fractal}}+O(R^{-1})$. Accordingly, we can determine the diffusion coefficient $\mathcal{D}_{\text{fractal}}$ by linear extrapolation in a plot of the right-hand member of (4.58) versus R^{-1}. These values are reported in Table II where we see the nice agreement with the values of the diffusion coefficient obtained by the other methods.

V. CONCLUSIONS

In the present paper, we investigated several consequences of dynamical chaos in the problem of diffusion in the conservative Lorentz gas. We considered open configurations of the Lorentz gas corresponding to experiments of scattering type. Our assumptions are completely consistent with the Liouville theorem of classical mechanics. We showed that the dynamics of the open Lorentz gas has properties of chaotic scattering that we characterize in terms of the escape rate, the Lyapunov exponent, the KS entropy, as well as the generalized fractal dimensions. On the microscopic level, the escape dynamics is controlled by a fractal repeller of trapped trajectories that forms the support of an invariant measure. The Liouvillian dynamics on this fractal admits a spectral decomposition in terms of the Pollicott-Ruelle resonances [35] that have been studied in closely related problems elsewhere [36,37]. The escape rate appears as the leading Pollicott-Ruelle resonance [6,8]. On the macroscopic scales, the escape dynamics is controlled by deterministic diffusion. By combining the microscopic and the macroscopic properties, we are able to relate the diffusion coefficient to the characteristic quantities of the chaotic and fractal repeller.

We can rephrase the previous considerations in the language of nonequilibrium statistical mechanics. The time scale associated with the Lyapunov exponent is the time scale where randomization occurs. This time scale corresponds to the kinetic time scale over which a local

equilibrium establishes itself. On the other hand, the hydrodynamical modes evolve on longer macroscopic time scales given by the inverse of the hydrodynamic rates like the diffusion rate $\gamma = \mathcal{D}k^2$ where k is the wave number. In the present work, we have studied the consequences of chaos on these long time scales. We considered diffusion as a scattering process in larger and larger scatterers. We showed that the finite size scatterers already presents kinetic irreversible properties like the escape rate. We have provided evidence for the fractal repeller which is the fundamental object at the origin of the kinetic properties and we calculated its Lyapunov exponent, KS entropy, and fractal dimensions. It is in the limit where the scatterer becomes large that the diffusionlike behavior emerges from the R^{-2} dependence of the escape rate.

In Sec. IV, we showed that the diffusion coefficient of the Lorentz gas can be obtained as a property of the scattering process of a point particle in open configurations. On the one hand, we calculated the diffusion coefficient in such scattering configurations by the first-passage method, the principle of which is based on the macroscopic phenomenology of diffusion.

On the other hand, we evaluated the diffusion coefficient from the Lyapunov exponent and the Hausdorff codimension of fractal repellers of increasing sizes according to our formula (4.58). This equation, which is the main result of the present paper, can be rewritten in the form

$$\mathcal{D} = \bar{\lambda}_e \lim_{R \to \infty} \left[\frac{R}{\chi_1} \right]^2 c_H(\mathcal{F}_R) , \tag{5.1}$$

in terms of the average Lyapunov exponent of the infinite lattice configuration of the Lorentz gas, since $\bar{\lambda}_e = \lim_{R \to \infty} \bar{\lambda}(\mathcal{F}_R)$. When the diffusion coefficient is not too small, the numerical values obtained with (5.1) ($\mathcal{D}_{\text{fractal}}$ in Table II) are in excellent agreement with the values obtained by the standard methods of Green-Kubo and of first-passage ($\mathcal{D}_{\text{GK}}$ and $\mathcal{D}_{\text{esc}}$ in Table II). This numerical agreement provides an important support to the chaotic-scattering theory of diffusion and to the validity of Eq. (5.1). Let us add that Eq. (5.1) can be rigorously proved for the multibaker model of deterministic diffusion [6].

Our results bring a very different understanding of diffusion. In conventional schemes, the understanding of diffusion is limited to the behavior of the system on macroscopic scales. With the chaotic-scattering theory of diffusion, we are able to understand that diffusion is compatible with a microscopic reversible dynamics that is volume preserving. This compatibility between the microscopic and macroscopic scales is realized because of the dynamical instability at the origin of chaos. Under nonequilibrium conditions like in the scattering configurations, the chaotic dynamics leads to the formation of a fractal object in phase space. The nonequilibrium invariant measure inherits of the fractal properties of the repeller and of the scattering process. Our results show the necessity of introducing such fractal and singular measures to describe the nonequilibrium properties in contrast to equilibrium statistical mechanics where smooth measures such as the Liouville measure are sufficient for most applications. We believe that these special properties of the nonequilibrium invariant measures are at the origin of the major difficulties encountered in nonequilibrium statistical mechanics since Boltzmann's classical works.

Dorfman and Gaspard have shown elsewhere how the chaotic-scattering theory can be applied not only to diffusion processes but also to other transport and reaction-rate processes [38]. On the other hand, Tasaki and Gaspard have proved in the multibaker model of diffusion that the fractal character of the repeller is intimately related to the fractallike and singular character of the diffusive eigendistributions associated with the Pollicott-Ruelle resonances of the Frobenius-Perron operator, as well as of the nonequilibrium invariant measures corresponding to constant concentration gradients [39]. In view of this set of consistent results, dynamical chaos and, in particular, chaotic scattering appear to provide a fundamental understanding of irreversible properties in terms of the symplectic dynamics of trajectories.

ACKNOWLEDGMENTS

It is our pleasure to thank Dr. G. Nicolis and Dr. M. Malek Mansour for encouragement and support in this research. We are grateful to J.-W. Turner who provided us with Ref. [30]. P. Gaspard gratefully acknowledges support from the National Fund for Scientific Research (F. N. R. S. Belgium). This research is supported, in part, by the Belgian Government under the program "Pôles d'Attraction Interuniversitaires" and the "Communauté Française de Belgique" under Contract No. ARC-93/98-166.

[1] D. J. Evans, E. G. D. Cohen, and M. P. Morris, Phys. Rev. A **42**, 5990 (1990).
[2] B. Moran and W. Hoover, J. Stat. Phys. **48**, 709 (1987).
[3] N. I. Chernov, G. L. Eyink, J. L. Lebowitz, and Ya. G. Sinai, Phys. Rev. Lett. **70**, 2209 (1993); Commun. Math. Phys. **154**, 569 (1993).
[4] P. Gaspard and G. Nicolis, Phys. Rev. Lett. **65**, 1693 (1990).
[5] P. Gaspard and F. Baras, in *Microscopic Simulations of Complex Hydrodynamic Phenomena,* edited by M. Maréschal and B. L. Holian (Plenum, New York, 1992), pp. 301–322.
[6] P. Gaspard, J. Stat. Phys. **68**, 673 (1992).
[7] P. Gaspard, in *From Phase Transitions to Chaos,* edited by G. Györgyi, I. Kondor, L. Sasvári, and T. Tél (World Scientific, Singapore, 1992), pp. 322–334.
[8] P. Gaspard, Chaos **3**, 427 (1993).
[9] P. Gaspard and S. A. Rice, J. Chem. Phys. **90**, 2225 (1989); **90**, 2242 (1989); **90**, 2255 (1989); **91**, 3279 (1989).
[10] J.-P. Eckmann and D. Ruelle, Rev. Mod. Phys. **57**, 617

(1985).
[11] C. Kittel, *Introduction to Solid State Physics* (Wiley, New York, 1976).
[12] Ya. G. Sinai, Russ. Math. Survey **25**, 137 (1970); L. A. Bunimovich, Commun. Math. Phys. **65**, 295 (1979); N. N. Krylov, *Works on the Foundations of Statistical Mechanics* (Princeton University Press, Princeton, NJ, 1979); Ya. G. Sinai, *ibid.*, p. 239; L. A. Bunimovich and Ya. G. Sinai, Commun. Math. Phys. **78**, 247 (1980); **78**, 479 (1980); L. A. Bunimovich, Ya. G. Sinai, and N. I. Chernov, Russ. Math. Surveys **45**, 105 (1990).
[13] P. Gaspard, in *Quantum Chaos,* Proceedings of the International School of Physics "Enrico Fermi", Course CXIX, Varenna, 1991, edited by G. Casati, I. Guarneri, and U. Smilansky (North-Holland, Amsterdam, 1993), pp. 307–383.
[14] V. I. Arnold and A. Avez, *Ergodic Problems of Classical Mechanics* (Benjamin, New York, 1968); I. P. Cornfeld, S. V. Fomin, and Ya. G. Sinai, *Ergodic Theory* (Springer, Berlin, 1982).
[15] B. Friedman, Y. Oono, and I. Kubo, Phys. Rev. Lett. **52**, 9 (1984).
[16] J.-P. Bouchaud and P. Le Doussal, J. Stat. Phys. **41**, 225 (1985).
[17] R. Bowen, *Equilibrium States and the Ergodic Theory of Anosov Diffeomorphisms,* Lecture Notes in Mathematics, Vol. 470 (Springer, Berlin, 1975).
[18] D. Ruelle, *Thermodynamic Formalism* (Addison-Wesley, Reading, MA, 1978).
[19] R. Bowen and D. Ruelle, Invent. Math. **29**, 181 (1975).
[20] P. Szepfalusy and T. Tél, Phys. Rev. A **34**, 2520 (1986); T. Tél, Phys. Lett. A **119**, 65 (1986); Phys. Rev. A **36**, 1502 (1987); T. Tél, J. Phys. A **22**, L691 (1989); Z. Kovács and T. Tél, Phys. Rev. Lett. **64**, 1617 (1990).
[21] T. Bohr and D. Rand, Physica D **25**, 387 (1987); T. Bohr and T. Tél, in *Directions in Chaos,* edited by U. Bai-lin Hao (World Scientific, Singapore, 1988), Vol. II, pp. 194–237; D. Bessis, G. Paladin, G. Turchetti, and S. Vaienti, J. Stat. Phys. **51**, 109 (1988).
[22] Ya. B. Pesin, Math. USSR Izv. **10**(6), 1261 (1976); Russ. Math. Surveys **32**(4), 55 (1977).
[23] H. Kantz and P. Grassberger, Physica D **17**, 75 (1985).
[24] P. Grassberger, R. Badii, and A. Politi, J. Stat. Phys. **51**, 135 (1988).
[25] H. Van Beijeren, Rev. Mod. Phys. **54**, 195 (1982).
[26] M. S. Green, J. Chem. Phys. **20**, 1281 (1952); **22**, 398 (1954); R. Kubo, J. Phys. Soc. Jpn. **12**, 570 (1957).
[27] J. Machta and R. Zwanzig, Phys. Rev. Lett. **50**, 1959 (1983); J. Stat. Phys. **32**, 555 (1983).
[28] L. P. Kadanoff and C. Tang, Proc. Natl. Acad. Sci. U.S.A. **81**, 1276 (1984).
[29] Chaos **3**, 417 (1993), focus issue on chaotic scattering, edited by E. Ott and T. Tél.
[30] L. Bauer and E. L. Reiss, SIAM J. Appl. Math. **35**, 508 (1978).
[31] T. C. Hasley, M. H. Jensen, L. P. Kadanoff, I. Procaccia, and B. I. Shraiman, Phys. Rev. A **33**, 1141 (1986).
[32] L. S. Young, Ergodic Theor. Dyn. Syst. **2**, 109 (1982).
[33] S. W. McDonald, C. Grebogi, E. Ott, and J. A. Yorke, Physica D **17**, 125 (1985).
[34] E. Ott, *Chaos in Dynamical Systems* (Cambridge University Press, Cambridge, England, 1993).
[35] M. Pollicott, Invent. Math. **81**, 413 (1985); D. Ruelle, Phys. Rev. Lett. **56**, 405 (1986); J. Stat. Phys. **44**, 281 (1986); J. Diff. Geom. **25**, 99 (1987); **25**, 117 (1987).
[36] P. Gaspard and D. Alonso Ramirez, Phys. Rev. A **45**, 8383 (1992).
[37] P. Cvitanović, P. Gaspard, and T. Schreiber, Chaos **2**, 85 (1992); P. Cvitanović, J.-P. Eckmann, and P. Gaspard, Chaos, Solitons, and Fractals (1995).
[38] J. R. Dorfman and P. Gaspard, Phys. Rev. E **51**, 28 (1995).
[39] S. Tasaki and P. Gaspard, in *Towards the Harnessing of Chaos,* edited by M. Yamaguti (Elsevier, Amsterdam, 1994), pp. 273–288; S. Tasaki and P. Gaspard (unpublished).